JAERI -M
83-192

DEVELOPMENT OF GAMMA-RAY DENSITOMETER AND MEASUREMENT OF VOID FRACTION IN INSTANTANEOUS PIPE RUPTURE UNDER BWR LOCA CONDITION

November 1983

Toshikazu YANO

日本原子力研究所
Japan Atomic Energy Research Institute

JAERI-M レポートは，日本原子力研究所が不定期に公刊している研究報告書です。

入手の問合わせは，日本原子力研究所技術情報部情報資料課（〒319—11 茨城県那珂郡東海村）あて，お申しこしください。なお，このほかに財団法人原子力弘済会資料センター（〒319—11 茨城県那珂郡東海村日本原子力研究所内）で複写による実費頒布をおこなっております。

JAERI-M reports are issued irregularly.

Inquiries about availabiljty of the reports should be addressed to Information Section, Division of Technical Information, Japan Atomic Energy Research Institute, Tokai-mura, Naka-gun, Ibaraki-ken 319—11, Japan.

編集兼発行　日本原子力研究所

印　　刷　㈱原子力資料サービス

JAERI-M 83-192

DEVELOPMENT OF GAMMA-RAY DENSITOMETER AND MEASUREMENT OF VOID FRACTION IN INSTANTANEOUS PIPE RUPTURE UNDER BWR LOCA CONDITION

Toshikazu YANO

Department of Nuclear Safety Research
Tokai Research Establishment, JAERI
(Received October 21, 1983)

In order to clarify the transient mass flow rate under the instantaneous pipe rupture condition, it is necessary to use a highly sensitive void meter. Therefore, a high-response gamma-ray densitometer was developed for the measurement of void fraction variation caused by flashing vaporization of the high-pressure and -temperature water under the instantaneous pipe rupture accident.

The measurement of void fraction was performed in the pipe rupture test under the BWR LOCA condition with a 6-inch diameter pipe. Initial conditions of the water were 6.86 MPa in pressure and the saturation temperature. To prove the reliability and accuracy, a calibration test by falling acrylic void simulators and an air injection test into cold water filled in the pipe were also conducted.

The following results are obtained in the pipe rupture test. (1) The cone slit method is very useful to increase the measuring accuracy. (2) It is clearly observed that the apparent increase of void fraction occurs after the rarefaction wave passes. (3) The first maximum of void fraction occurs with some delay time after break. The following minimum void fraction concurs with the maximum pressure in the pressure recovering phenomena and with the maximum blowdown thrust force.

Keywords: Gamma-ray, Densitometer, Three Beams, BWR, LOCA, Frashing, Pipe Rupture, Measurement, Void Fraction, Accuracy, Mass Flow Rate

---

The work was performed under contract with the Atomic Energy Bureau of Science and Technology Agency of Japan.

JAERI−M 83−192

ガンマ線密度計の開発およびBWR・LOCA条件下の配管瞬時破断時のボイド率計測

日本原子力研究所東海研究所安全工学部
矢野歳和

（１９８３年10月21日受理）

配管の瞬時破断時の過渡的な流出流量を明らかにするためには高感度のボイド計が必要である。そこで配管瞬時破断時の高温高圧水のフラッシングによるボイド率変化を計測するために高応答のガンマ線密度計を開発した。

ボイド率変化の計測はＢＷＲ・ＬＯＣＡ条件下での６インチ口径管による配管破断試験において実施した。高温高圧水の初期条件は6.86 MPaの飽和水である。また,ガンマ線密度計の信頼性と精度を明らかにするため，アクリル製の模擬ボイドによる落下試験と冷水が満たされた配管の中に空気を吹き込んで較正試験をも実施した。

配管破断試験でのボイド率計測から以下の結論を得た。

(1) ガンマ線密度計の計測精度を上げるためには，円錐状のスリットを用いる方法は非常に有効である。

(2) 配管の瞬時破断時に配管内を膨張波が通過した後にボイド率が急激に増加する現象が確認できた。

(3) 破断後のボイド率の最初の極大値はある遅れ時間の後に生じる。次にボイド率の極小値は圧力回復現象での圧力の極大値およびブローダウン推力の最大値と同時刻に生じる。

この報告書は，電源開発促進対策特別会計法に基づき，科学技術庁からの受託研究，昭和56年度配管信頼性実証試験のジェット放出試験に関し，γ線密度計を開発し試験した結果をまとめたものである。

CONTENTS

目　　次

1. INTRODUCTION

An instantaneous pipe break is one of the hypothetical accidents of the light water reactor (LWR). The restraints are installed in the pipe lines of nuclear power plants to stop the dynamic movement of the piping which is called "pipe whip". To analyze such an interaction between the whipping pipe and restraints under the loss of coolant accident (LOCA), it is necessary to study the time histories of the blowdown thrust force, "loading function". It is important to investigate the blowdown thrust force from the thermalhydraulic view point.

A high-response void meter will be useful to examine the transient flashing flow of the coolant water after the instantaneous pipe rupture. There are many methods for measuring the void fraction[1][2]. An atenuation method is suitable to detect the flashing fluid inside the non-transparent pipe which is made of a low-carbon steel or stainless steel pipe under the high-pressure and -temperature conditions. For this purpose a gamma-ray or X-ray densitometer is applicable for the void fraction measurement.

In the present experiment, a gamma-ray densitometer is selected for the measurement of the coss-sectional average density. However, there are few experimental studies concerning the initiation of flashing vaporization for the instantaneous pipe break. This paper shows the time-dependent void fraction both just after the instantaneous pipe break and during the quasi-steady blowdown in the jet discharge tests under the boiling water reactor (BWR) LOCA condition[3].

2. VOID FRACTION BY A GAMMA-RAY DENSITOMETER

Figure 1 shows the basic conceptional arrangement of a gamma-ray densitometer. The gamma-ray intensity after the attenuation, I, is generally expressed as

$$I = I_o \exp\left[-\sum_{i=1}^{n} (\sigma_i \gamma_i d_i)\right] \tag{1}$$

where, I_o, σ, γ, d are the intensity injected to the pipe surface, the reaction cross-section of gamma-ray, the specific weight and the distance of attenuation substance, respectively.

The relationship between the average void fraction α and the apparent specific weight γ_a for the flashing two-phase flow is shown as follows;[1][2]

$$\gamma = \alpha \gamma_g + (1 - \alpha)\gamma_\ell \tag{2}$$

The value of γ can be obtained by a gamma-ray densitometer.

If the intensity of gamma-ray before the pipe rupture is known, the specific weight in the blowdown phenomena can be obtained by Eq. (3).

$$\gamma(t) = \gamma_{in} - \frac{1}{\sigma_{H_2O} \cdot d} \cdot \ln\left(\frac{I(t)}{I_{in}}\right) \tag{3}$$

Therefore, if the initial conditions of the fluid is known, the void fraction in a certain stage of two-phase flow can be expressed as follows;

$$\alpha(t) = \frac{1}{\gamma_\ell(t) - \gamma_g(t)} \left\{\gamma_\ell(t) - [\alpha_{in}\gamma_{g,in} + (1-\alpha_{in})\gamma_{\ell,in}] + \frac{1}{\sigma_{H_2O} \cdot d} \cdot \ln\left(\frac{I(t)}{I_{in}}\right)\right\} \tag{4}$$

When the initial fluid is the non-flashing water, α_{in} is equal to zero. Therefore, Eq. (4) becomes

$$\alpha(t) = \frac{1}{\gamma_\ell(t) - \gamma_g(t)} \left\{\gamma_\ell(t) - \gamma_{in} + \frac{1}{\sigma_{H_2O} \cdot d} \cdot \ln\left(\frac{I(t)}{I_{in}}\right)\right\} \tag{5}$$

3. METHOD OF MEASUREMENTS

3.1 Design of gamma-Ray Densitometer

The gamma-ray densitometer is composed of a gamma-ray source cask and a detector box. The densitometer has three beems to detect the void fraction of two-phase flow in the steel pipe.

Figure 2 shows the details of the source cask of the gamma-ray densitometer. Photographs 1 and 2 show the source cask. The densitometer in this experiment has a gamma source of ^{137}Cs which is enclosed in the welded stainless steel capsule.

Figure 3 and Photo. 3 show the gamma-ray source and the source capsule, respectively. The intensity of the source is about 10 curies.

The source cask for gamma-ray shield is composed of lead and tungsten alloy. Stainless steel is used for the containment structure. The outer wall of the cask is 10 mm in thickness and the inner pipe for the structures of movable shield is 1½ in × sch 160, respectively.

Figure 4 and Photo. 4 show the movable shield attaching the air piston. The gamma-ray source can be moved and stored by an air piston.

Photographs 5 and 6 show the cone-slit attachment produced by the lead mounted on the gamma-source cask shown in Fig. 2. To irradiate the test pipe, the gamma source is moved to the desired position where three long cone-slits are bored in the lead shielding. The angle of a cone slit is 4°20', and each of three slits is holed each other at some distance, where the angle is about 6°30'.

Photographs 7 and 8 show the detector box, in which three scintillators and pre-amplifiers are mounted. Each channel of three gamma-ray beams can be measured by three NaI(Tℓ) scintillators. A scintillator is 38.1 mm in diameter and 50.8 mm in length. The dimensions and arrangement are designed to collect completely the dispersed gamma-ray beams through the opened cone slit.

Figure 5 shows the arrangement of the gamma-ray densitometer mounted on the stand in the jet discharge test[3]. To increase the efficiency of the gamma-ray detection, the distance between the gamma-source and scintillation detectors was designed to be as close as possible. The source cask and detector box were manufactured to be as close as possible.

Photographs 9 and 10 show the water cooling jackets which have double walls for cooling. The gamma-ray source cask and detector box

were covered by the water cooling jacket to avoid the temperature increase by the blowdown steam. Furthermore, the cooling air was supplied to the detector box for the protection against the temperature increase of scintillators.

The counting rate, r, of the gamma-particle is shown[4] in Eq. (6).

$$r = r^{*} \pm \frac{1}{n^{\frac{1}{2}}} \tag{6}$$

The counting error caused by the statistical deviation of the gamma source decay is shown as $\pm 1/n^{\frac{1}{2}}$.

The relative error depending on the measuring systems of the gamma-ray is also shown as follows.

$$\frac{\sigma_I}{I} = \left(\frac{q}{2\ I\ RC}\right)^{\frac{1}{2}} \tag{7}$$

where R and C are the individual constant of feedback circuit for the detector. As shown in Eq. (7), in order to decrease the error by the statistical decay of the gamma-ray source, it is necessary to get more couting rates in the measurement if a gamma-ray source is given or its intensity is limited.

The response characteristics of the detector could be optionally chosen by the selection of the amplifier switches which was conducted by changing the combination of R and C for the time constant of the electrical circuit. The relative errors of the present systems were 4.3 % when the response of detectors was selected for 1 KHz range, and 1.4 % for 100 Hz, respectively.

3.2 Calibration Tests

3.2.1 Calibration Test by falling Acrylic Void Simulator

Before the blowdown experiment, the response of the gamma-ray densitometer must be examined in the cold state before heating-up. Therefore, falling tests were conducted using acrylic void simulators to confirm the efficiency of the gamma-ray densitometer.

Figure 6 and Photo. 11 show the apparatus for the calibration test. Photographs 12 through 14 show the acrylic void simulator. The simulator was 85 mm in diameter and 100 mm in height. The void fraction of the

acrylic simulator was decided by adjusting the volume of cylindrical holes. The falling speed was measured by the time difference which was detected by the void simulator obstructing photo-beam between two positions.

Figure 7 shows the time sequence of the falling void simulator and the conceptual signal having the delay time cuased by the response of detection circuit. The time history of the output signal is obtained as the reverse trapezoid shape. This is caused by the delay time between the arrival of the void simulator at the edge of cone-shape radiation beam and the complete covering of the whole beam. Therefore, it is not due to the low response of the measuring system itself.

Figures 8 and 9 show the typical results of the falling test by acrylic void simulators.

Figure 10 shows several results of falling test by varing the void fraction. The falling speed of the void simulator was 3.9 m/sec in the experiment. The period passing through the radiation beam calculated by the falling speed of void simulator is 32.3 msec. This duration shows a good agreement with the experimental time and there is no time delay in the detection as shown in Fig. 10. In this case, the falling speed of the void simulator is relatively slow. Therefore, there is little difference in the time delay between the predicted time history of gamma-ray intensity and the experimental signal as shown in Fig. 7 and Fig. 10.

Moreover, it is proved that the obvious difference during three type void simulators can be recognized, and it is confirmed that the gamma-ray densitometer has a higher response than 1 KHz and the ability for the measurement of flashing vaporization.

3.2.2 Calibration Test by injecting Air into Pipe filled with Cold Water

Air injection tests were performed to prove the efficiency under the real void variation in which the air was injected into the cold water. The flow rate of air was variously changed to get the different flow paterns.

Photographs 15 and 16 show the typical results of bubbly flow and slug flow, respectively. Figure 11 shows the time-dependent voltage output of the gamma-ray densitometer when the recurrent air slug is passing inside the stainless steel pipe. Here, the density variation can be obtained clearly, and it is confirmed that the transient measurement for void fraction can be examined in the cold water test.

3.3 Jet Discharge Test by Instantaneous Pipe Rupture

The gamma-ray densitometer was used for the pipe rupture test with a 6-inch pipe under the BWR LOCA conditions[3]. This test was performed for the study of the discharged jet, in which the blowdown thrust and jet impingement forces were examined by the load cells and evaluated by the measured thermalhydraulic quantities.

Figure 12 shows a schematic diagram of the jet discharge test, and Table 1 shows the test conditions. The initial conditions of the hot water were 6.86 MPa in pressure and the saturation temperature. Photograph 17 shows the test apparatus. Photograph 18 shows the arrangement of the gamma-ray densitometer on the stand. The void fraction was measured at 652 mm from the rupture disk or at 911 mm from the pipe exit. The initial water level in the pressure vessel was 4 m in height. A guillotine break was simulated by the break of a rupture disk with an electric arc.

This pipe rupture test was already reported as Run 5608[3], in which the thermalhydraulic quantities were shown in detail.

4. RESULTS AND DISCUSSION

4.1 Experimental Correction of the Void Fraction

Figure 13 shows the pressure hisotires of the instantaneous pipe break under the BWR LOCA conditions. Figures 14 through 25 show the gamma-ray intensity vs. time of three beams named XU201 through XU203 in the experiment. The time ranges are 0.1, 1, 5 and 50 second, respectively. Judging from the pressure signal at the break exit, the time origin of pipe rutpure is 33 ms on the figures. Figure 26 shows a typical result of the gamma-ray intensity for the center channel of the three beams, XU202. The voltage output can be converted into the specific weight by Eq. (3).

However, many factors exist in the measurement errors. They are the couting efficiency of the detector, the displacement of pipe between gamma-source and detectors differing from the initial setting, the thermal expansion or contraction of the test pipe, and others.

Therefore, the calibrations for the detector systems must be conducted. If the correction constant, C_d, is introduced for the detection errors, the calibrated attenuation distance, d^*, is defined as follows.

$$d^* = C_d \cdot d_o \tag{8}$$

where, d_o is the real distance of the gamma-ray attenuation.

If the initial and end conditions of the fluid are known, the following equation is given by Eq. (3).

$$d^* = \frac{\ln (I_{end}/I_{in})}{\sigma_{H_2O} \cdot (\gamma_{in} - \gamma_{end})} \tag{9}$$

In the present experiment, the quantities for calculation of the void fraction are shown in Table 3. For example of the center channel, CH2 (XU202), it is obtained by Eq. (9) that d^* is equal to 0.130 m. The original attenuation distance, d_o, is equal to 0.1288 m for the center gamma beam, which is the inner diameter of 6-inch pipe. Therefore, C_d is obtained by eq. (8).

$$C_d = d^*/d_o = 1.02 \tag{10}$$

This means that the real error in the present measuring system exists within 2 per cent, and the reliability and accuracy of the gamma-ray densitometer are proved.

When the rarefaction wave propagates from the broken exit into the hot water, the rapid vaporization will generate in the hot water called "flashing". The relationship between the void fraction and quality is shown as follows;

$$\alpha = 1/\{1 + (\frac{1-x}{x}) \frac{\gamma_g}{\gamma_\ell} \cdot K\} \tag{11}$$

$$x = K/\{K + (\frac{1-\alpha}{\alpha}) \cdot \frac{\gamma_\ell}{\gamma_g}\} \tag{12}$$

where the slip ratio K is defined as

$$K \equiv \frac{u_g}{u_\ell} = \frac{x}{1-x} \cdot \frac{1-\alpha}{\alpha} \cdot \frac{\gamma_\ell}{\gamma_g} \tag{13}$$

It is difficult to determine the slip K in the flashing initiation. If the flashing flow is assumed to be homogeneous under the thermal equilibrium condition, $\gamma_\ell(t)$ and $\gamma_g(t)$ in Eq. (5) can be represented by the densities of the saturation condition, $\gamma_{\ell,sat}$ and $\gamma_{g,sat}$, which are obtained by the observed pressure history and its saturation temperature. The void fraciton and quality in the homogeneous flow are shown in Eqs. (14) and (15), in which K is equal to one.

$$\alpha = \frac{\gamma_{\ell,sat}(t) - \gamma(t)}{\gamma_{\ell,sat}(t) - \gamma_{g,sat}(t)} \tag{14}$$

$$x = 1/\{1 + (\frac{1-\alpha}{\alpha}) \cdot \frac{\gamma_\ell}{\gamma_g}\} \tag{15}$$

Furthermore, the void fractin weighted by cross-sectional area S for three beams can be obtained for three beam densitometer by Eqs. (16) through (18).

$$\alpha' = \sum_{i=1}^{n} (\eta_s \cdot \alpha)_i$$

$$= \eta_{s,1} \cdot \alpha_1 + \eta_{s,2} \cdot \alpha_2 + \eta_{s,3} \cdot \alpha_3 \tag{16}$$

$$C_w = \frac{1}{\sum_{i=1}^{n} \eta_{s,i}} = \frac{1}{(S_1/S) + (S_2/S) + (S_3/S)} \tag{17}$$

$$\alpha = C_w \cdot \alpha' \tag{18}$$

where, C_w is the weighting correction coeffcient of the gamma-ray beam crossing the test pipe. The quality weighted by the area crossing the beams inside the pipe can be obtained by the same procedure as mentioned above. Figure 27 shows three beams of gamma-ray crossing the test pipe, and Table 4 shows the calibration coefficient and the results.

4.2 Void Fraction and Quality under Instantaneous Pipe Rupture Conditions

Figure 28 shows the histories of the void fraction and quality. The time range are 0.1, 1.0 and 50 sec, respectively. Figures 28 (a) and (b) show the void fraction and quality just after the instantaneous pipe break at the location of 652 mm from the rupture point. Comparing the pressure history with the void fraction between Fig. 13 and Fig. 28, the apparent increase of void fraction occurs at about 10 ms after the rarefaction wave passes inside the test pipe. The delay time of flashing vaporization is caused by both the delay time of flashing itself and the break opening time of rupture disk.

The first maximum of the void fraction or the quality occurs at about 60 msec, when the void fraction is equal to 0.41 or the quality is equal to 0.026, respectively. It is considered that the first increase of the void fraction is cuased by the increase of the discharged mass flow near the broken exit, and by the flashing vaporization. The thermal non-equilibrium state is relaxed during the flashing vaporization, which is initiated by the superheated water with the existence of the nuclei for the bubble growth. However, the void fraction becomes lower after the first maximum according as the increase of the mass flow and the pressure recovery of the thermal non-equilibrium relaxation.

The minimum void fraction occurs at 0.25 sec after the pipe break and the value is equal to 0.25, when the quality by the homogeneous model is equal to 0.014. This is due to the fact that the minimum void

fraction or quality occurs with some delay time after the pipe break. At first, the initial flow from the broken exit is discharged by the pressure and enthalpy difference between the pipe and ambient environment and the mass flow is considered to increase. The void fraction increases with the increase of discharged mass. Secondary, the non-equilibrium relaxiation is recovered by the flashing vaporization in the superheated water and the system pressure of the fluid near the exit reaches the extreme maximum value. Thereafter, the equilibrium stage is obtained when the system pressure recovers the maximum value and the void fraction or quality reaches the minimum one. Furthremore, it is confirmed that the mass flow rate also reaches the maximum as it was analysed in the PWR LOCA conditions[5].

In general, the time when the first maximum void fraction is obtained differs at each location. The first maximum void fraction propagates from the broken exit to the inner of the pipe with some delay time. If the distance between a certain location of the test pipe and the pipe exit becomes shorter, the first maximum void fraction becomes larger. This tendency was proved in the analysis of the PWR LOCA conditions[5].

4.3 Blowdown Thrust Force

Figure 29 shows the time history of blowdown thrust force[3]. It is shown that the maximum force concurs with the minimum void fraction at 0.25 sec after break.

To evalute the blowdown thrust force from the experimental results under the instantaneous pipe rupture, the folloiwng time-dependent quantities must be obtained. These are the mass flow rate, specific weight and exit pressure of the fluid in the momentum equation[5].

To obtain the mass flow rate for two-phase mixtures such as that in the blowdown conditions, two measuring conbinations are needed. For example, a gamma densitometer is used for detecting the specific weight and a drag disk for detecting the momentum flux of the two-phase flow[1]. In addition, if the pressures of the broken pipe are measured in the experiment, the blowdown thrsut force can be evaluated by the momentum equation. Therefore, the present gamma-ray densitometer having the high-responsibility is very useful to evaluate the blowdown thrust force.

5. CONCLUSIONS

To investigate the mass flow rate under th instantaneous pipe rupture conditions of the LWR, a gamma-ray densitometer was developed and examined for the void fraction measurement. The following conclusions are obtained.

(1) The detection method of void fraction by using a cone-type slit for a gamma-ray beam and a large scintillator is very useful to increase the measuring accuracy of the gamma-ray densitometer. This method is also useful to examine the average void fraction in the cross-section of pipe.

(2) The gamma-ray densitometer shows good reliabilities and high responce in the calibration test by falling acrylic void simulators and test by injecting air into the pipe filled with cold water.

(3) It is recognized that the apparent increase of the void fraction is caused by the flashing vaporization under th instantaneous pipe break conditions after the rarefaction wave passes.

(4) The measurements by the gamma-ray densitometer also show that the void fraction or quality reaches the first maximum value after the instantaneous pipe break. However, according as the pressure recovery, the void fraction or quality attains to the minimum when the maximum pressure concurs. Afterwards, the void fraction or quality increases gradually with the increase of the discharged fluid from the pipe.

ACKNOWLEDGEMENTS

The author wishes to make his acknowledgement to Dr. S. Miyazono, Mr. T. Isozaki, Mr. R. Kato, the members of the pipe rupture project group, Mr. N. Sasamoto, Mr. S. Tanaka, Dr. Y. Koizumi, Dr. Y. Anoda, Dr. M. Sobajima, Mr. H. Murata and Mr. T. Wakabayashi at the Japan Atomic Energy Research Institute for their fruitful discussions, and the Oyo-Koken Co. for the manufacturing of apparatus and assistance in calibration tests. He also wishes his thanks to Mr. H. Oura at the Nuclear Engineering Co. and the KURS Co. for their helpful assitance in the experiments.

This work was performed under contract with the Atomic Energy Bureau of Science Technology Agency of Japan to demonstrate the safety for pipe rupture of the primary coolant circuits in nuclear power plants.

References

[1] J. Reimann, J. John and U. Müller, Measurements of Two-Phase Mass Flow Rate: A Comparison of Different Techniques, Int. J. Multiphase Flow, Vol. 8, No. 1 (1982) 36-46.

[2] U. Müller, T. Kobayashi and T. Saito, Measurements of Mass Flow Rate for Two-Phsae Flow, JSME, Vol. 84, No. 784 (1981) 13-18.

[3] T. Yano, T. Isozaki, N. Miyazaki, S. Ueda, R. Kurihara, R. Kato and S. Miyazono, An Experimental Study of Blowdown Thrust and Jet Forces by 6-Inch Pipe under BWR LOCA, The 2nd International Topical Meeting on Nuclear Reactor Thermal-Hydraulics, Santa Barbara, California, U.S.A., January 11-14, 1983, Thermal-Hydraulics of Nuclear Reactor, Vol. 2, published by Ame. Nucl. Soc. (1983) 761-768.

[4] W.J. Price, Nuclear Radiation Detection (McGraw-Hill Book Co. 1964).

[5] T. Yano, N. Miyasaki and T. Isozaki, Transient Analysis of Blowdown Thrust Force under PWR LOCA, Nuclear Engineering and Design, Vol. 75, No. 1 (1982) 157-168.

ACKNOWLEDGEMENTS

The author wishes to make his acknowledgement to Dr. S. Miyazono, Mr. T. Isozaki, Mr. R. Kato, the members of the pipe rupture project group, Mr. N. Sasamoto, Mr. S. Tanaka, Dr. Y. Koizumi, Dr. Y. Anoda, Dr. M. Sobajima, Mr. H. Murata and Mr. T. Wakabayashi at the Japan Atomic Energy Research Institute for their fruitful discussions, and the Oyo-Koken Co. for the manufacturing of apparatus and assistance in calibration tests. He also wishes his thanks to Mr. H. Oura at the Nuclear Engineering Co. and the KURS Co. for their helpful assitance in the experiments.

This work was performed under contract with the Atomic Energy Bureau of Science Technology Agency of Japan to demonstrate the safety for pipe rupture of the primary coolant circuits in nuclear power plants.

References

[1] J. Reimann, J. John and U. Müller, Measurements of Two-Phase Mass Flow Rate: A Comparison of Different Techniques, Int. J. Multiphase Flow, Vol. 8, No. 1 (1982) 36-46.

[2] U. Müller, T. Kobayashi and T. Saito, Measurements of Mass Flow Rate for Two-Phsae Flow, JSME, Vol. 84, No. 784 (1981) 13-18.

[3] T. Yano, T. Isozaki, N. Miyazaki, S. Ueda, R. Kurihara, R. Kato and S. Miyazono, An Experimental Study of Blowdown Thrust and Jet Forces by 6-Inch Pipe under BWR LOCA, The 2nd International Topical Meeting on Nuclear Reactor Thermal-Hydraulics, Santa Barbara, California, U.S.A., January 11-14, 1983, Thermal-Hydraulics of Nuclear Reactor, Vol. 2, published by Ame. Nucl. Soc. (1983) 761-768.

[4] W.J. Price, Nuclear Radiation Detection (McGraw-Hill Book Co. 1964).

[5] T. Yano, N. Miyasaki and T. Isozaki, Transient Analysis of Blowdown Thrust Force under PWR LOCA, Nuclear Engineering and Design, Vol. 75, No. 1 (1982) 157-168.

Table 1 Experimental conditions in jet discharge test

Run No.	:	5608
Test Type	:	Jet Discharge
Test Conditions	:	PWR LOCA
Test Pipe	:	6 inch
Inner Diameter	:	128.8 mm
Initial Pressure	:	6.86 MPa
Initial Temperature		
Pressure Vessel	:	283 DEG-C
Test pipe	:	279 DEG-C
Break Area Ratio	:	86.5 %

Table 3 Quantities for calculation of void fraction and quality, Run 5608

QUANTITIES				REMARKS
σ_{H_2O}	= 8.96 x 10^{-3}	m^2/kg	:	Gamma-rry, 661 keV, ^{137}Cs
γ_{in}	= 751.2	kg/m^3	:	Water, 6.86 MPa, 279 DEG-C
γ_{end}	= 0.5977	kg/m^3	:	Steam, 0.10 MPa, 100 DEG-C
I_{in}	= 0.268	Volt	:	CH.1 (XU201), Initial Output
I_{end}	= 0.589	Volt	:	CH.1 (XU201), End Output
I_{in}	= 0.349	Volt	:	CH.2 (XU202), Initial Output
I_{end}	= 0.844	Volt	:	CH.2 (XU202), End Output
I_{in}	= 0.369	Volt	:	CH.3 (XU203), Initial Output
I_{end}	= 0.716	Volt	:	CH.3 (XU203), End Output

Table 2 Measuring conditions of gamma-ray densitometer, Run 5608

Test No,	Tag. No.		XU201	XU202	XU203
	Channel No.		CH 1	CH 2	CH 3
	Position		South	Center	North
EMPTY PIPE				2 Dec. 1981	
	Amp.	Range	I	II	III
		Gain	7.43	3.42	10.00
		Time Const.	II	II	II
		Zero	0.23	0.20	0.16
	Closed		-0.002 V	0.005 V	0.009 V
1	Open	Pipe only	0.898 V	0.884 V	0.550 V
2		Pipe + 20mmAl	0.595 V	0.595 V	0.390 V
3		Pipe + 4mmAl	0.803 V	0.787 V	0.500 V
WATER FILLED PIPE ..... Room Temp., 7 Dec. 1981					
	Amp.	Range	I	II	III
		Gain	7.43	3.42	2.65
		Time Const.	II	II	II
		Zero	0.23	0.20	0.16
	Closed		-0.003 V	0.005 V	0.015 V
4	Open	Pipe + Water	0.325 V	0.380 V	0.422 V
	WATER FILLED PIPE ..... Room Temp., 7 Dec. 1981				
	Amp.	Range	I	II	II
		Gain	7.43	3.42	7.76
		Time Const.	III	III	III
		Zero	0.17	0.23	0.18
	Closed		0.000 V	0.000 V	0.000 V
5	Open	Pipe + Water	0.335 V	0.379 V	0.324 V
	EXPERIMENTAL RESULTS			8 Dec. 1981	
	Amp.	Range	I	II	II
		Gain	7.43	3.42	7.76
		Time Const.	III	III	III
		Zero	0.17	0.23	0.18
	Closed 12:56		0.011 V	0.039 V	0.013 V
6	Open 12:58 51 kg/cm^{2}G		0.337 V	0.460 V	0.497 V
	Amp. 13:21	Range	---	---	5.30
		Zero	---	---	0.18
	Closed 13:21		0.001 V	0.002 V	0.003 V
7	Open before Test 13:23 68 kg/cm^{2}G		0.312 V	0.433 V	0.413 V
8	Run 5608 13:47 from output	Before break	0.268 V	0.349 V	0.369 V
		50 sec after break	0.589 V	0.844 V	0.716 V

Table 4 Weighting coefficient for void fraction

RUN 5608

Channel No.	1	2	3
Tag. No.	XU201	XU202	XU203
Position	South	Center	North
Area of gamma-ray crossing the pipe, S_i	25.3 cm^2	28.1 cm^2	21.9 cm^2
Area ratio by the total area, $\eta_{s,i}=S_i/S$	0.194	0.216	0.168
Attenuation distance under the calibration d_i	118.5 mm	131.3 mm	98.6 mm
Remarks (Run No. 5608)	6 inch pipe × Sch 160, STS42 128.8mmϕI.D., 165.2mmϕO.D. 18.2 mmt Total area S = 130.2 cm^2 $(S_1/S)+(S_2/S)+(S_3/S)$ = 0.578 Weighted coefficient for void fraction $C_w = \frac{1}{0.578} = 1.73$		

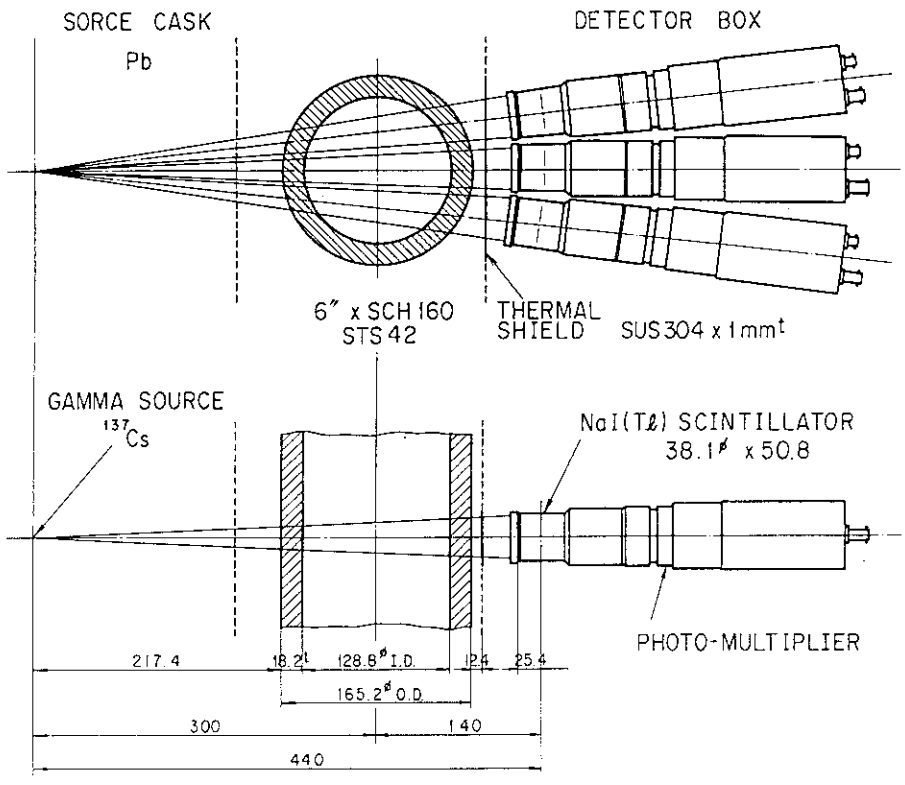

Fig. 1 Basic conceptional arrangement of three beam gamma-ray densitometer

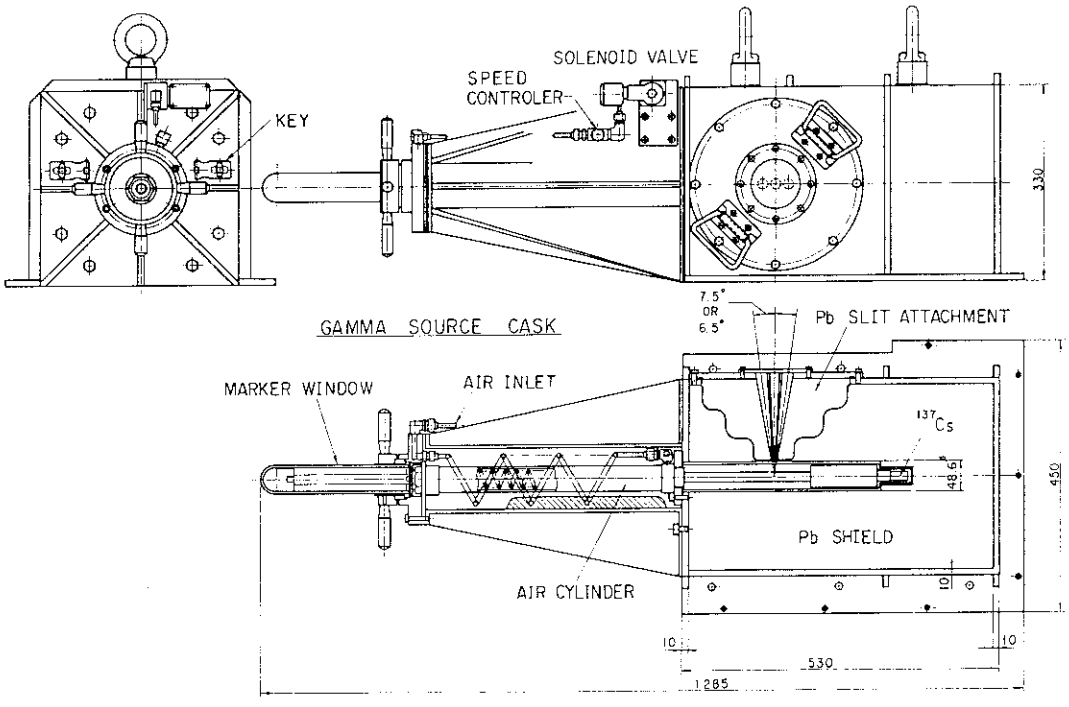

Fig. 2 Details of source cask

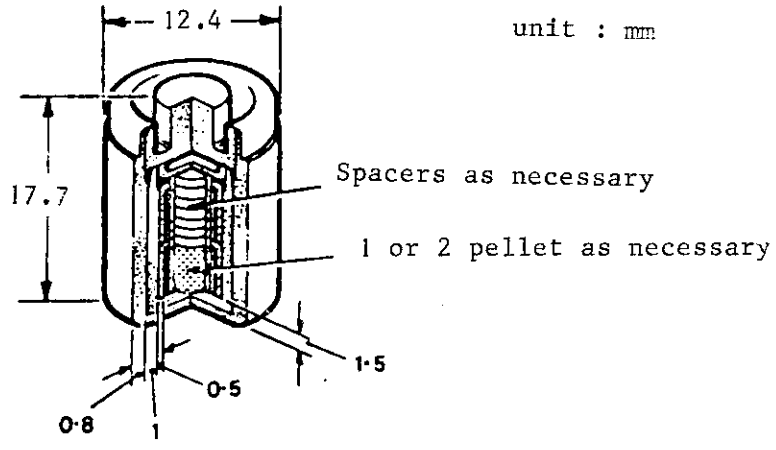

X.60/2 10 Ci Type CDC6025

Fig. 3 Gamma-ray source in closed capsule using a ^{137}Cs isotope pellet

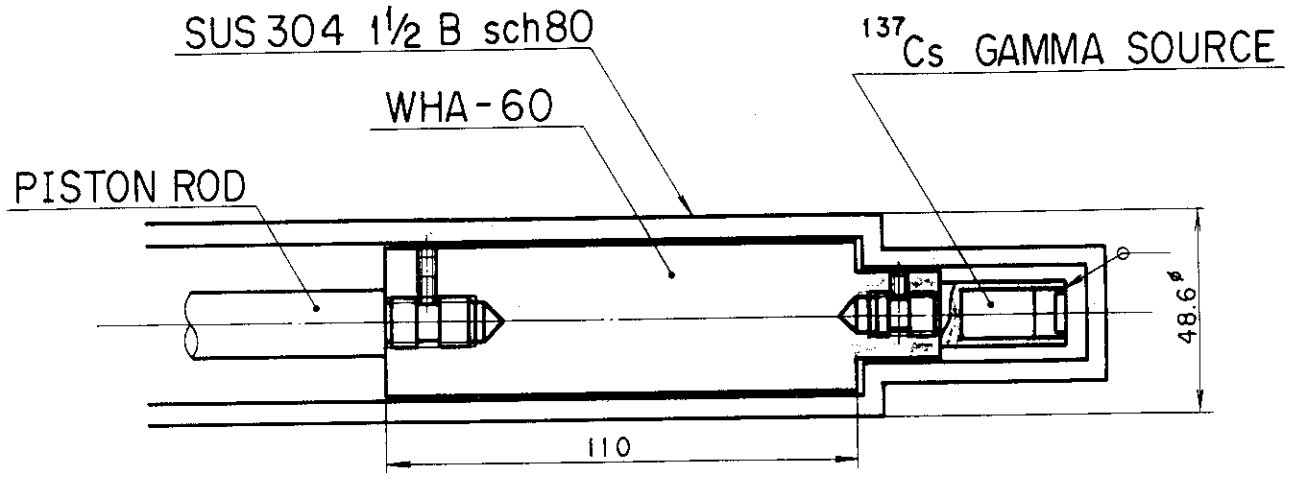

Fig. 4 Movable shield of gamma-ray source

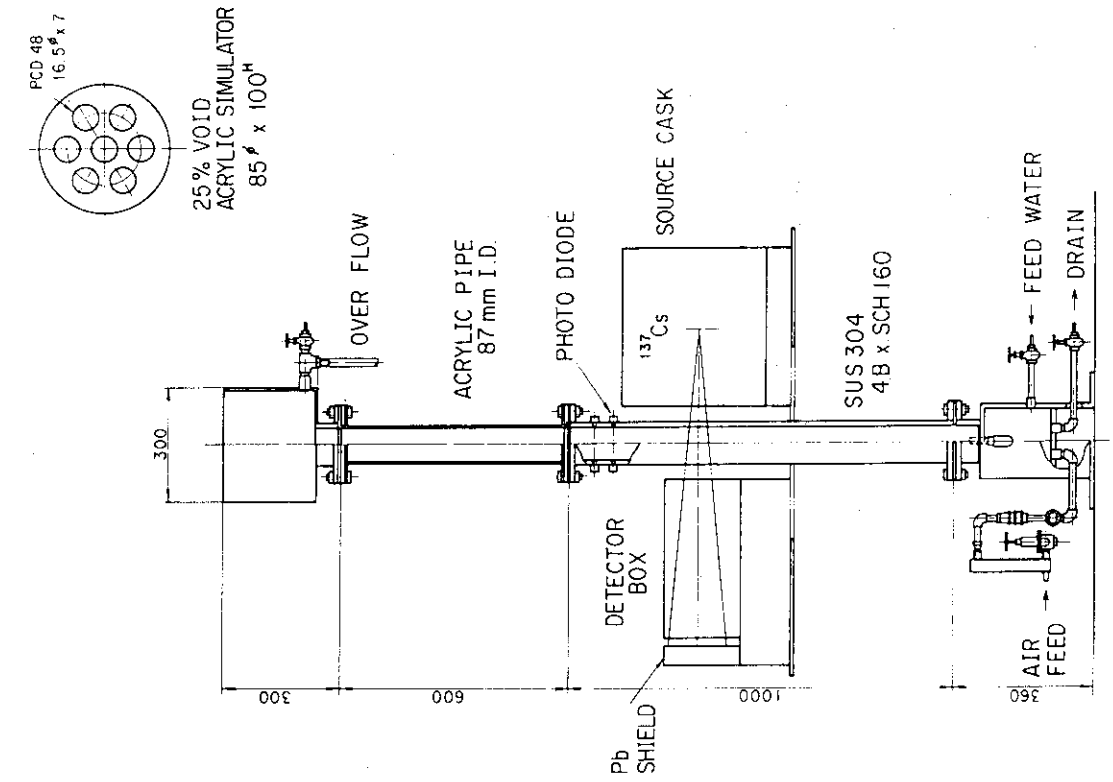

Fig. 6 Calibration apparatus

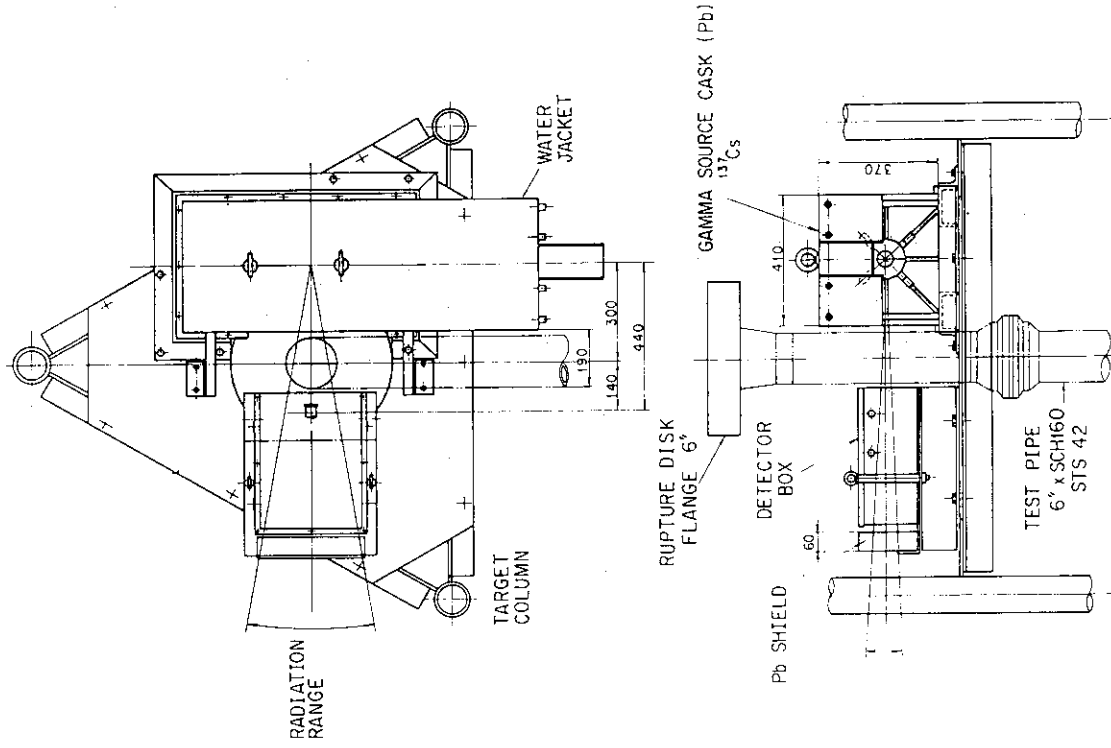

Fig. 5 Arrangement of source cask and detectors

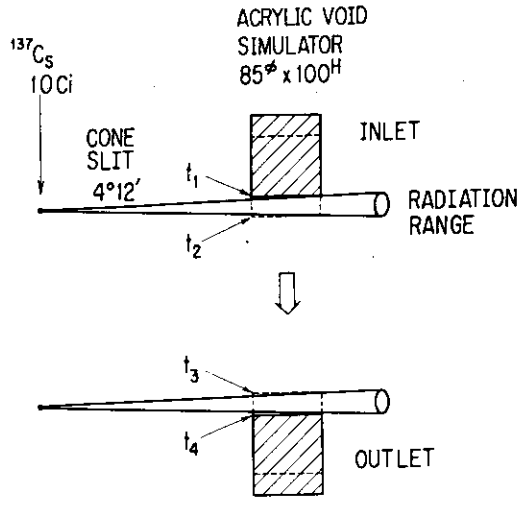

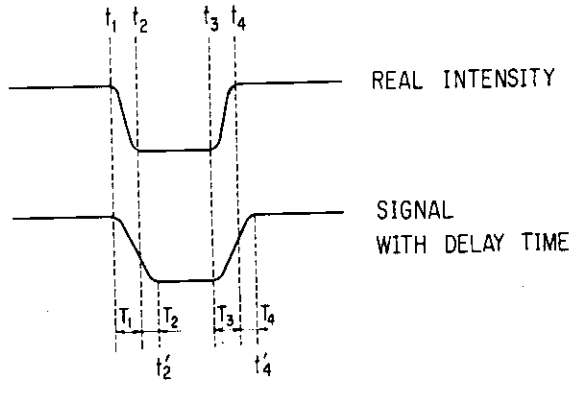

Fig. 7 Time sequence of falling test using void simulators

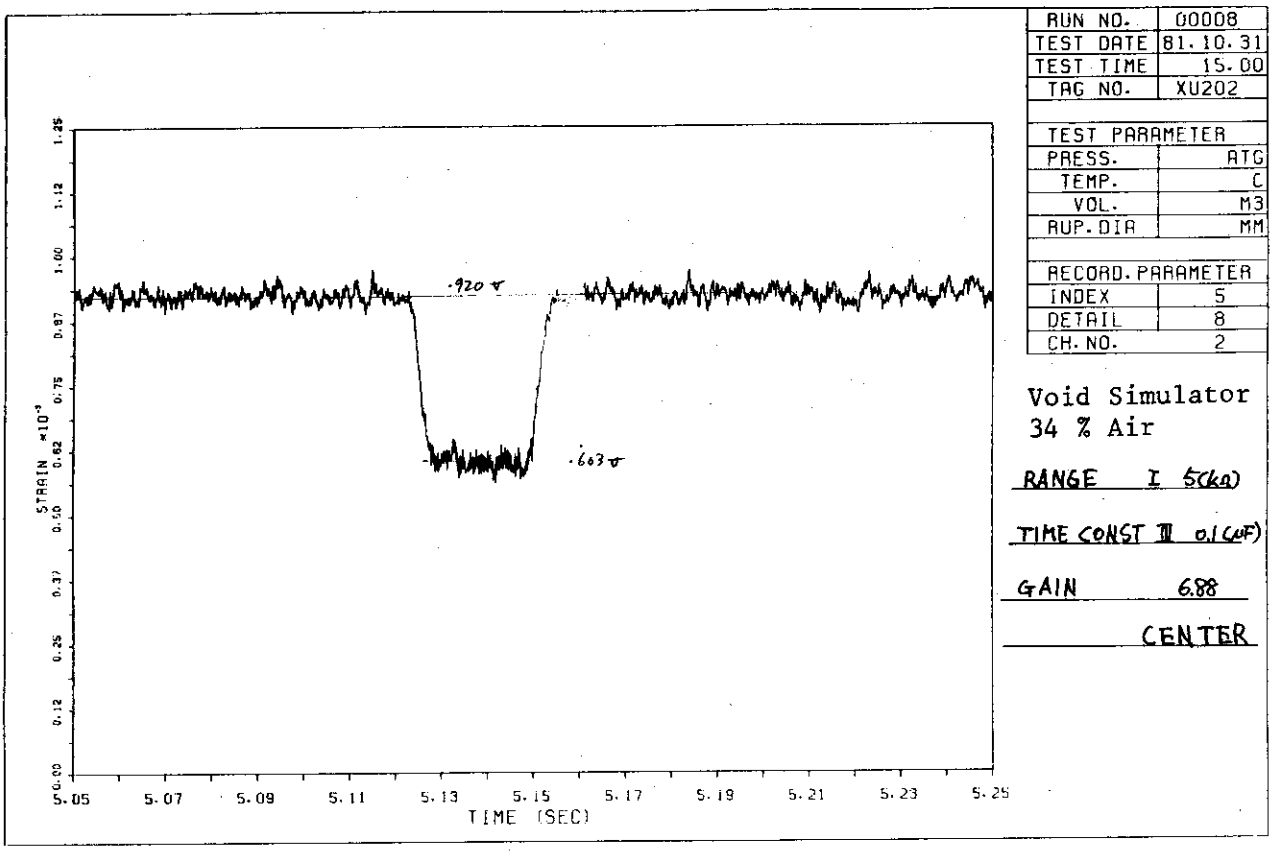

Fig. 8 Falling test by 34% air simulator

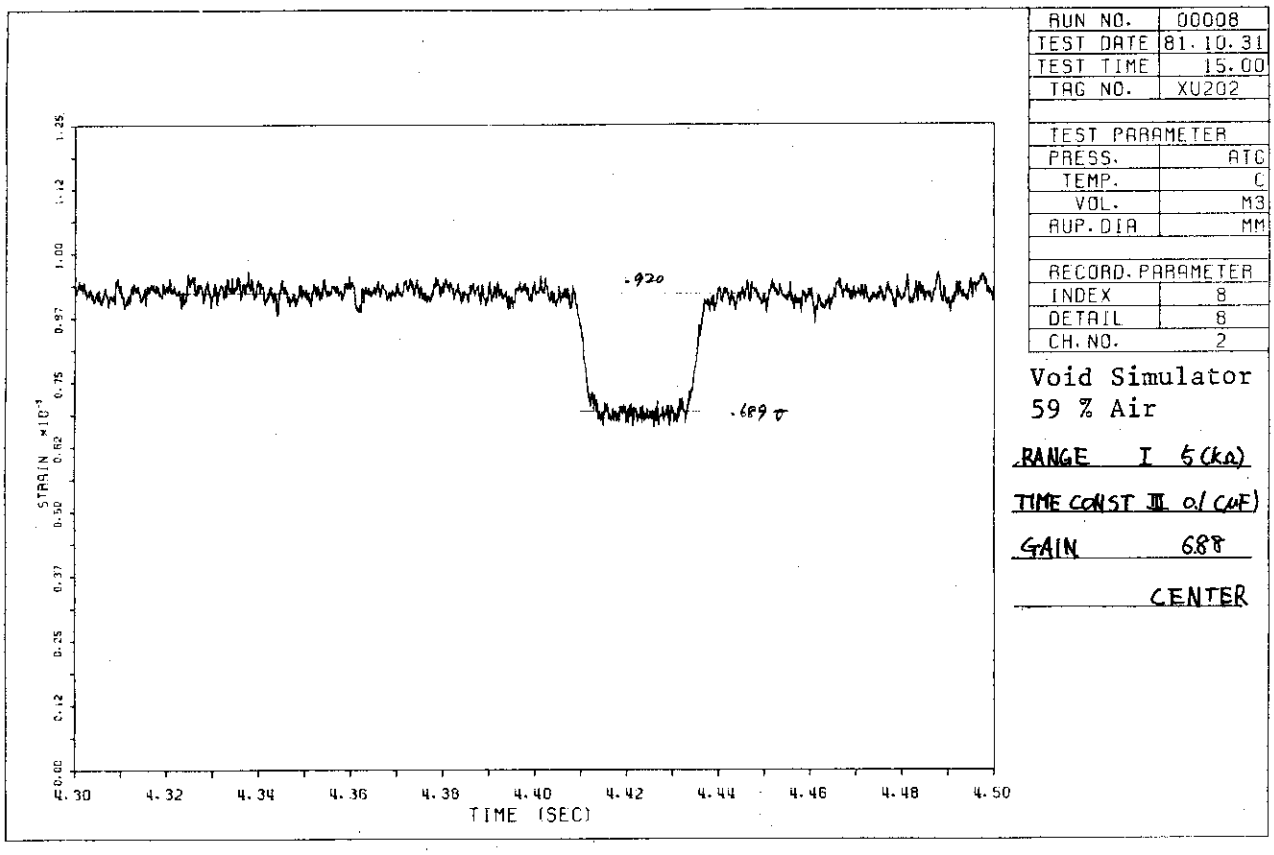

Fig. 9 Falling test by 59% air simulator

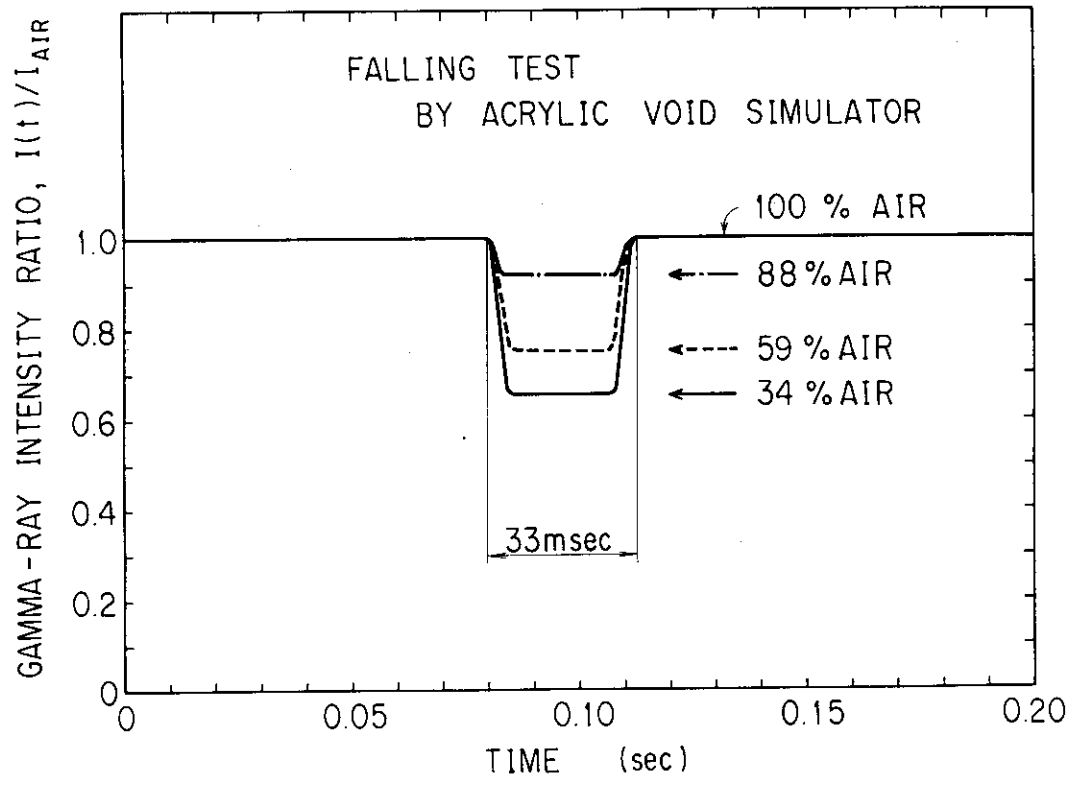

Fig. 10 Experimental results of falling test with void simulators

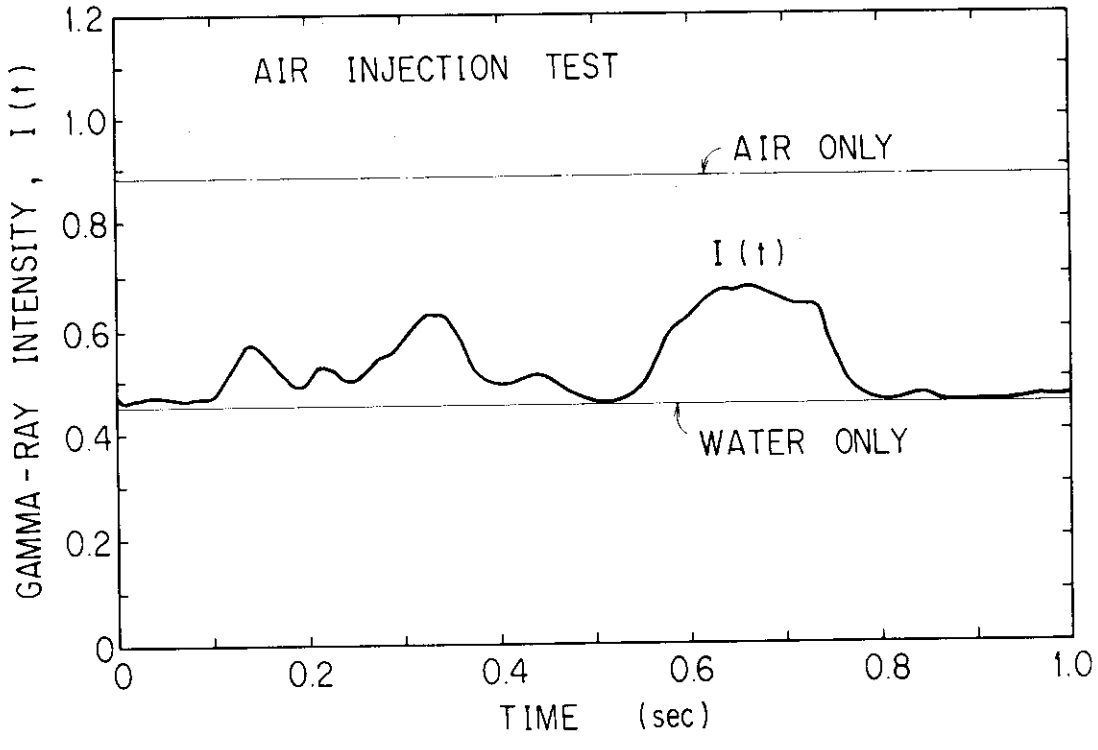

Fig. 11 Experimental results of gamma-ray intensity in the air injection test

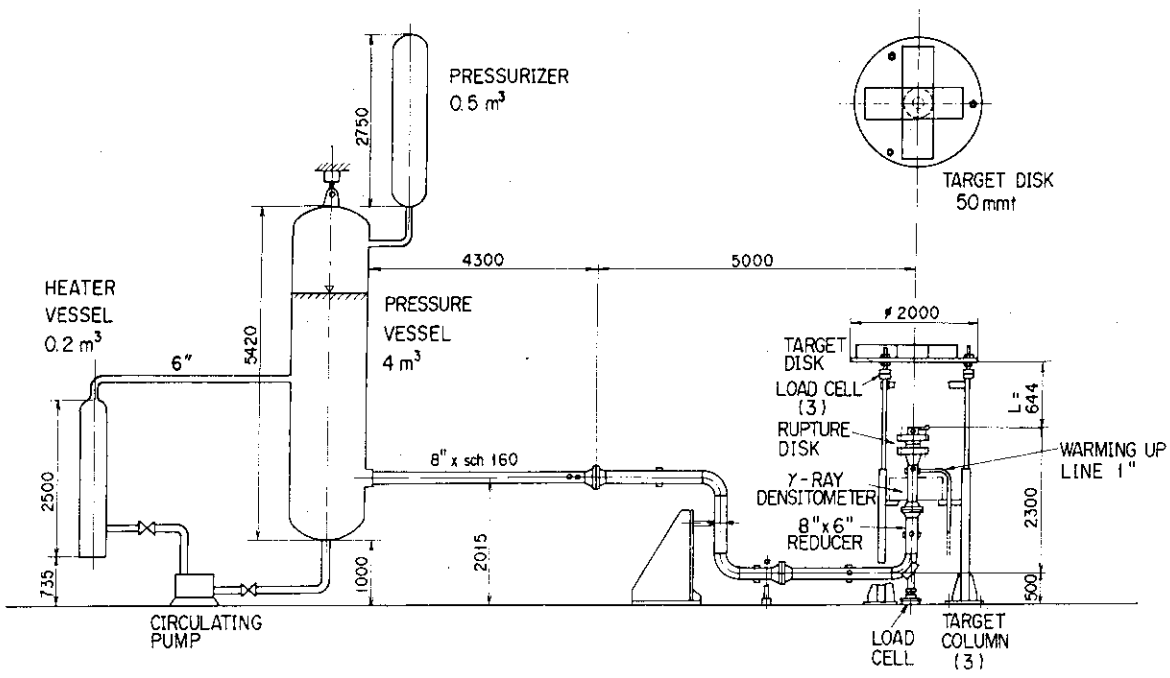

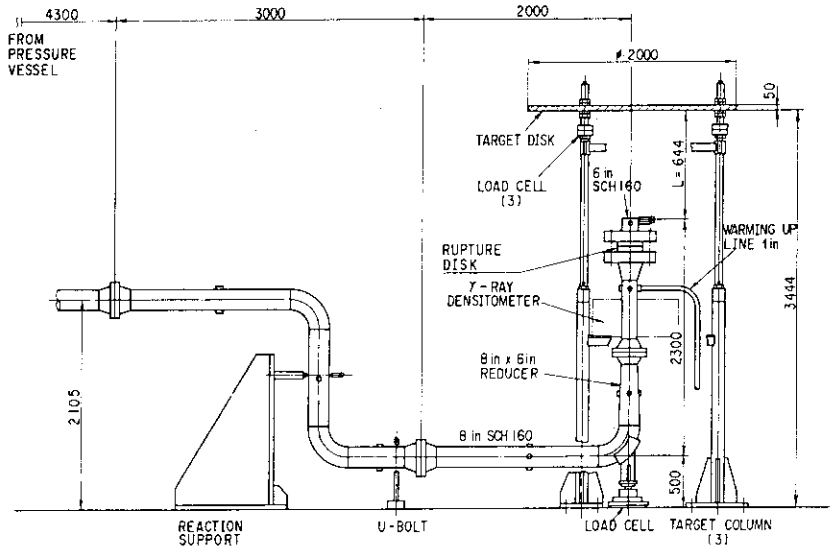

Fig. 12 Facility of jet discharge test

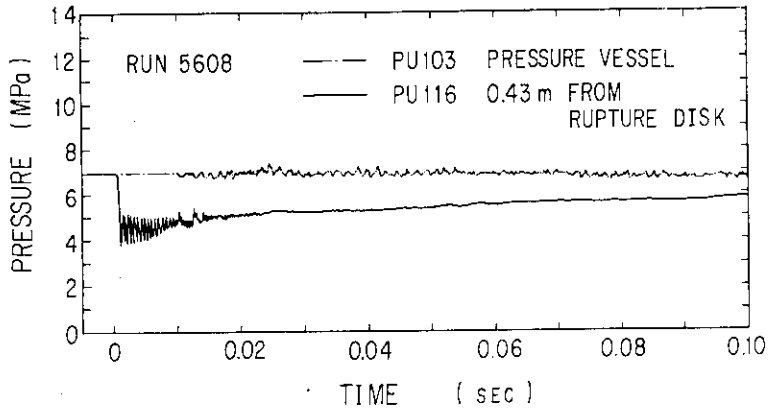

(a) 0 - 0.1 sec

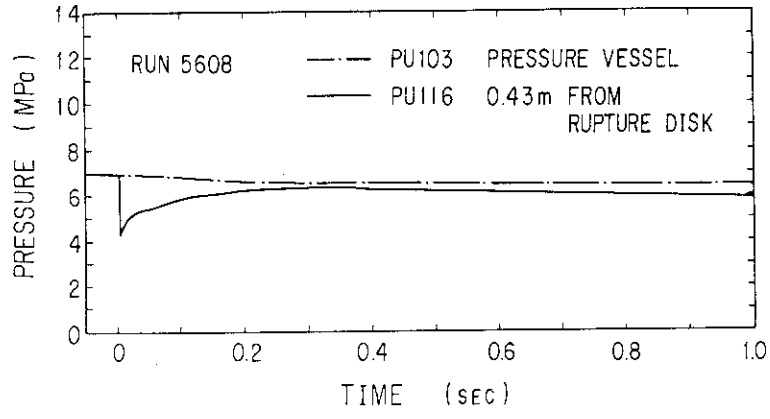

(b) 0 - 1 sec

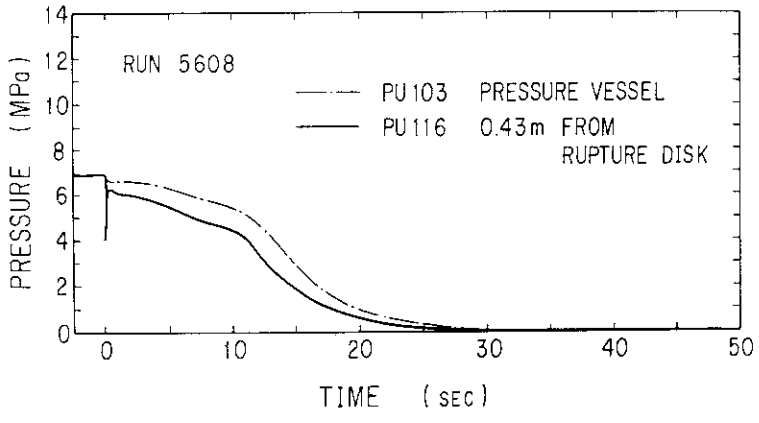

(c) 0 - 50 sec

Fig. 13 Pressure histories in jet discharge test

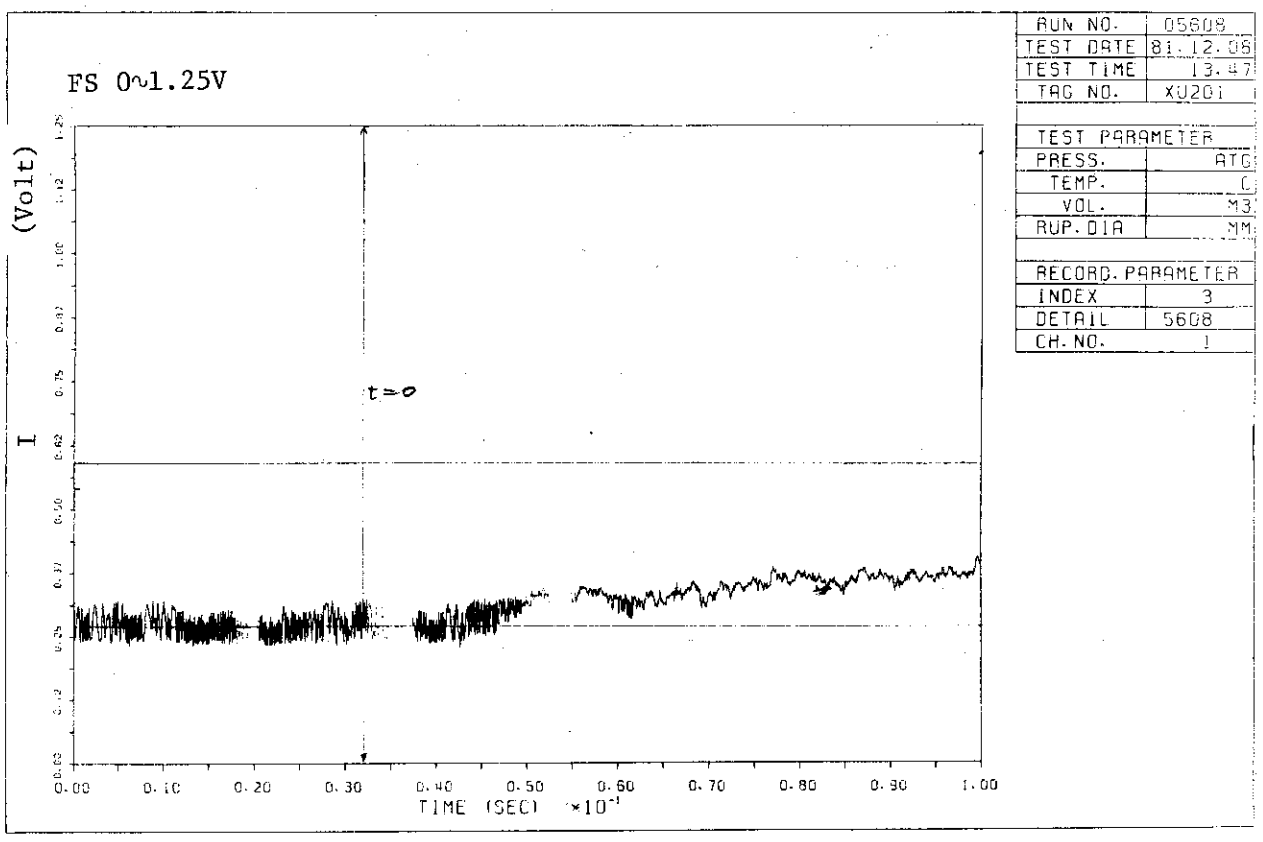

Fig. 14 Output of gamma-ray densitometer, Run 5608, XU201, 0 - 0.1 sec

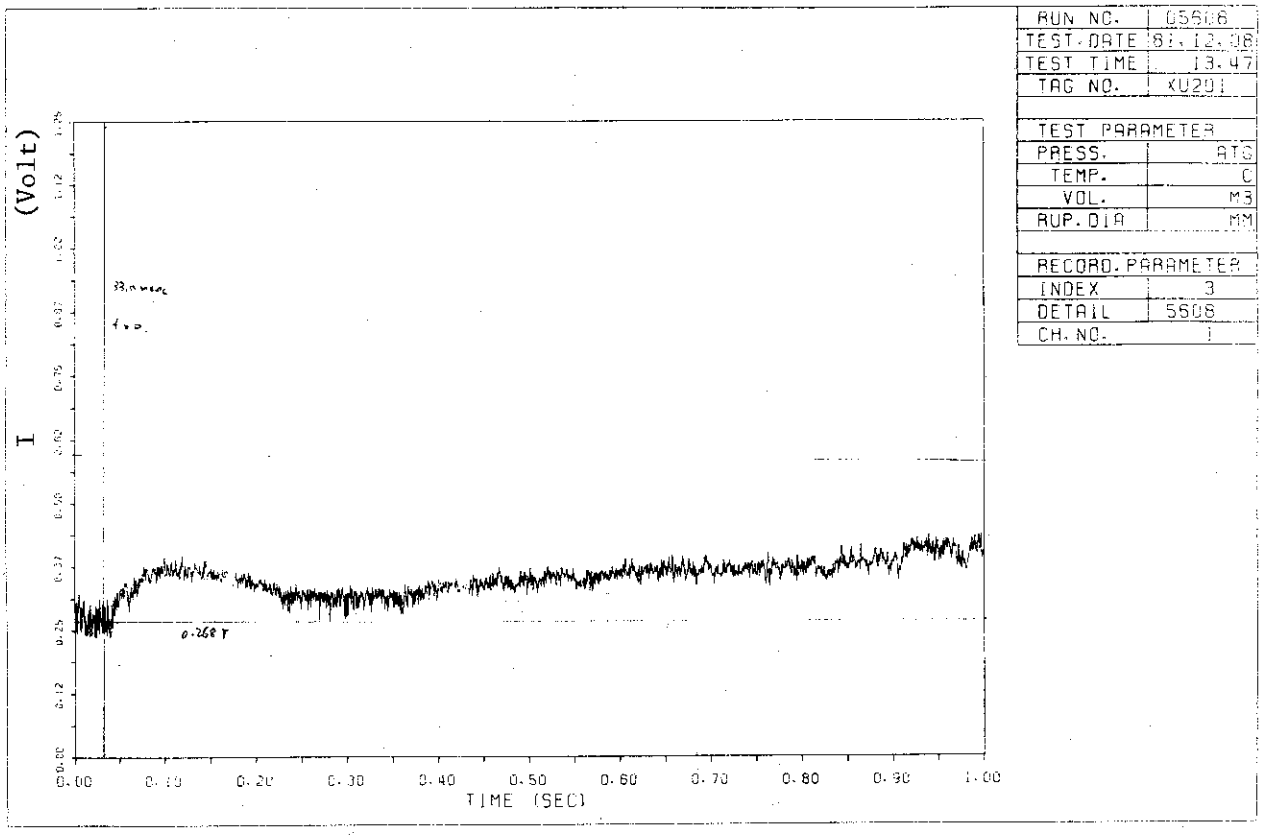

Fig. 15 Output of gamma-ray densitometer, Run 5608, XU201, 0 - 1 sec

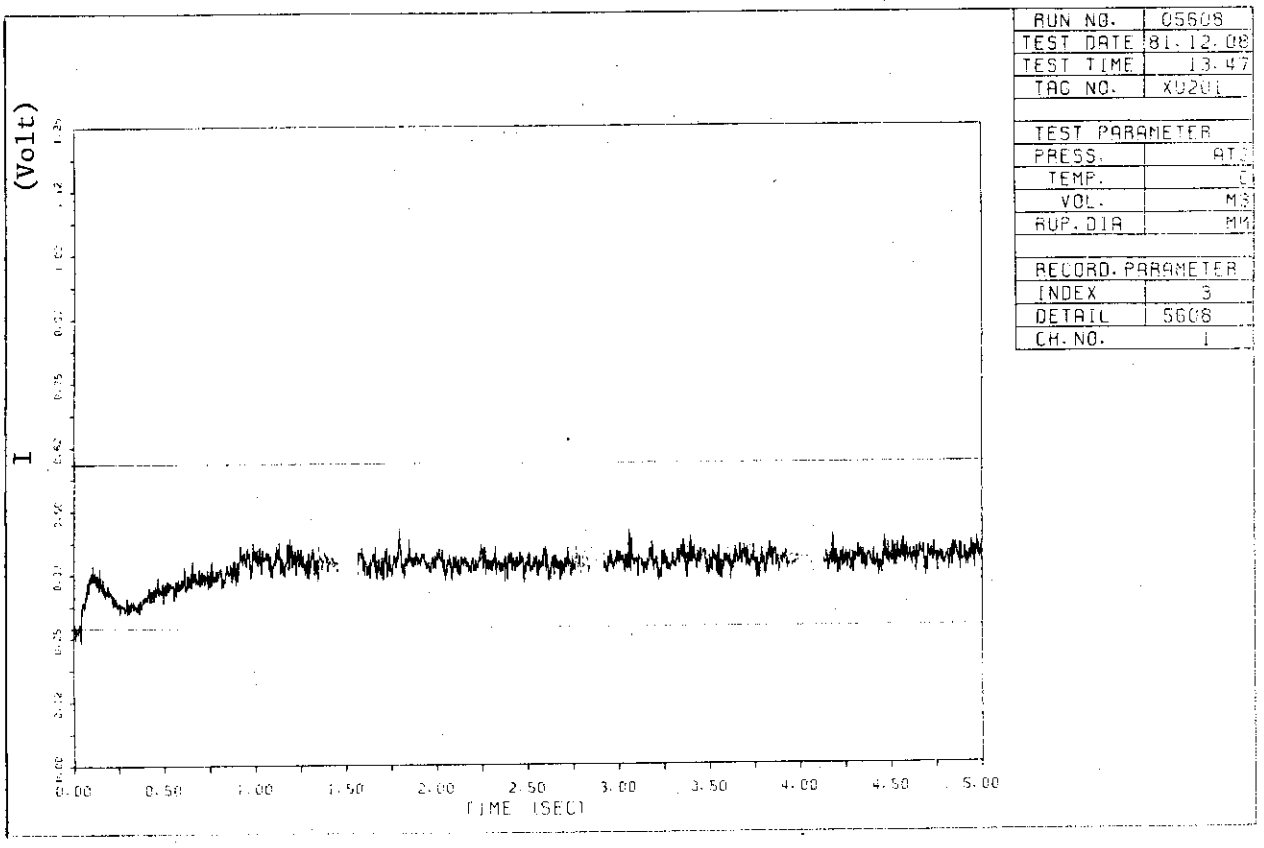

Fig. 16 Output of gamma-ray densitometer, Run 5608, XU201, 0 - 5 sec

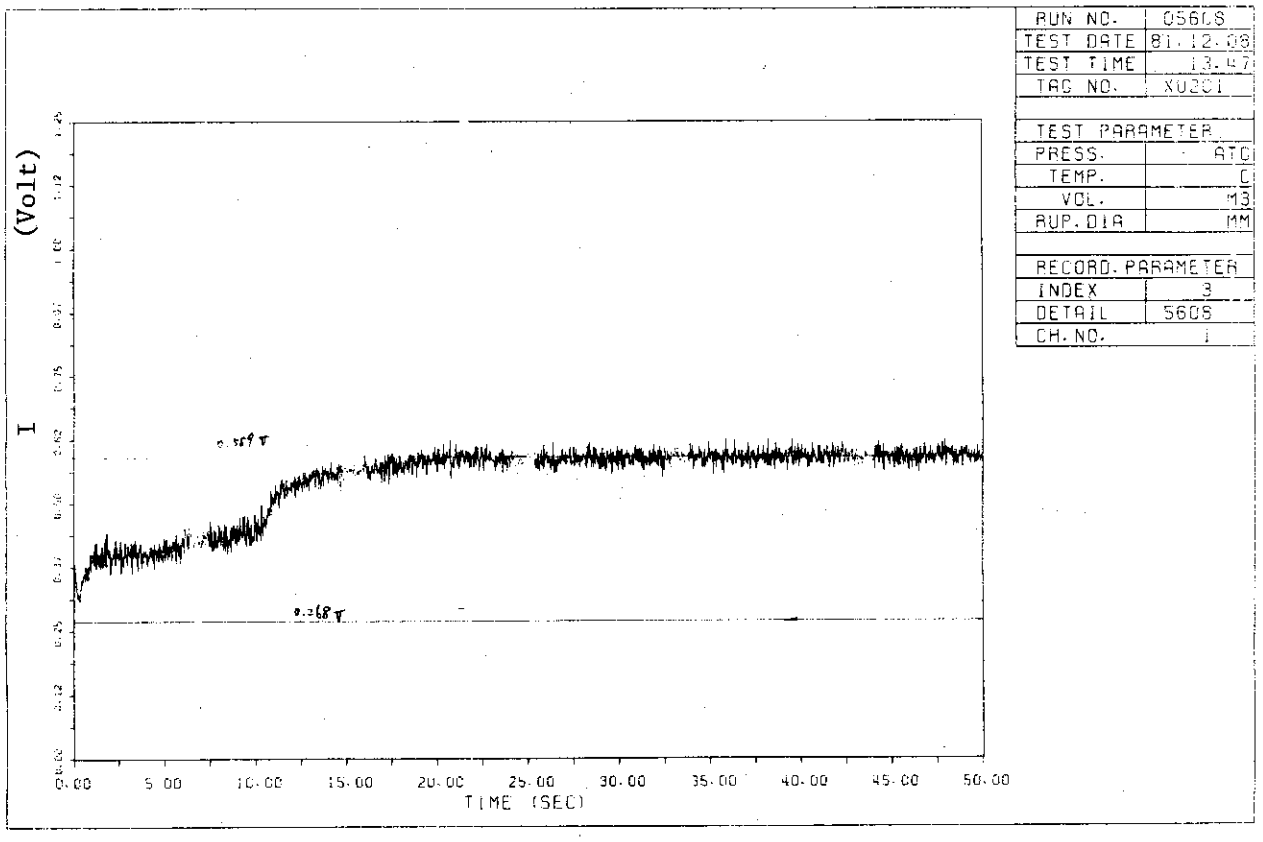

Fig. 17 Output of gamma-ray densitometer, Run 5608, XU201, 0 - 50 sec

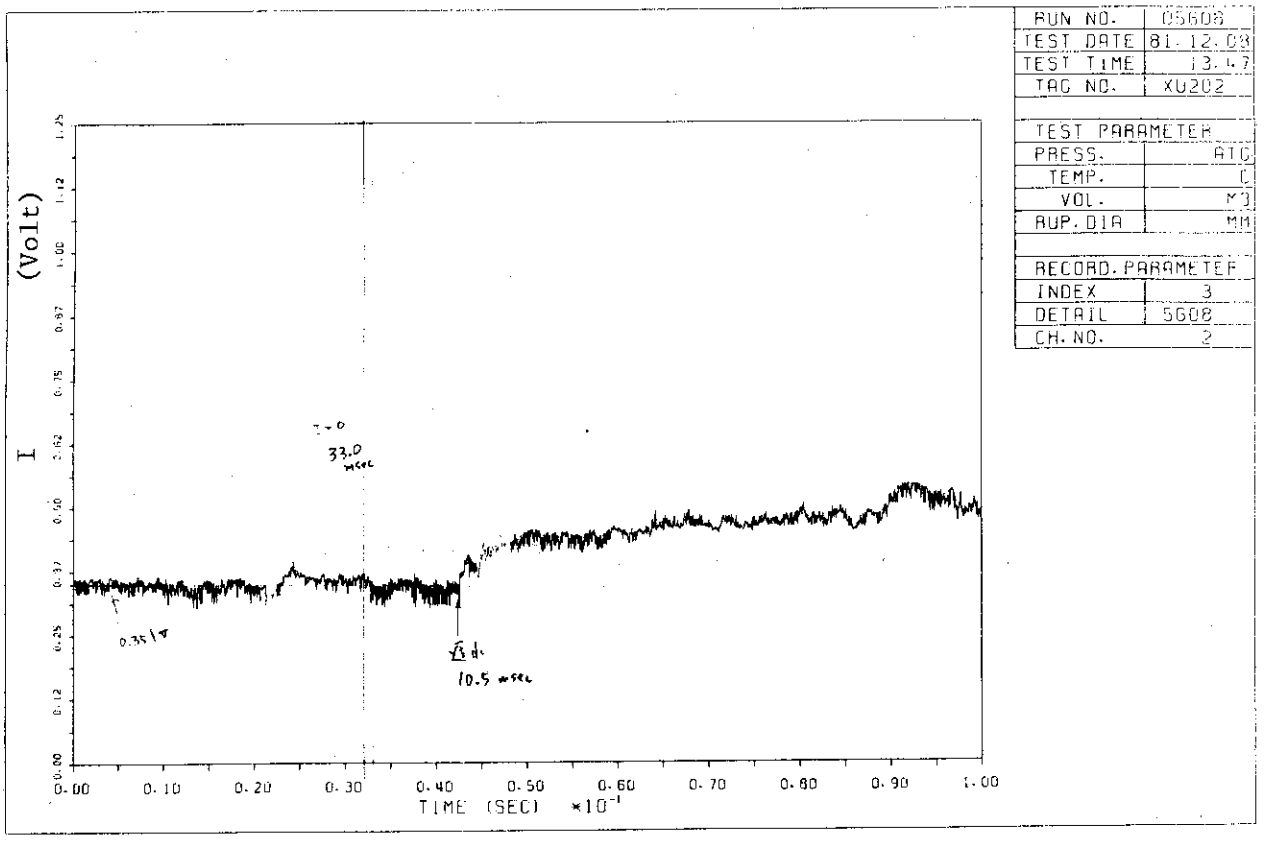

Fig. 18 Output of gamma-ray densitometer, Run 5608, XU202, 0 - 0.1 sec

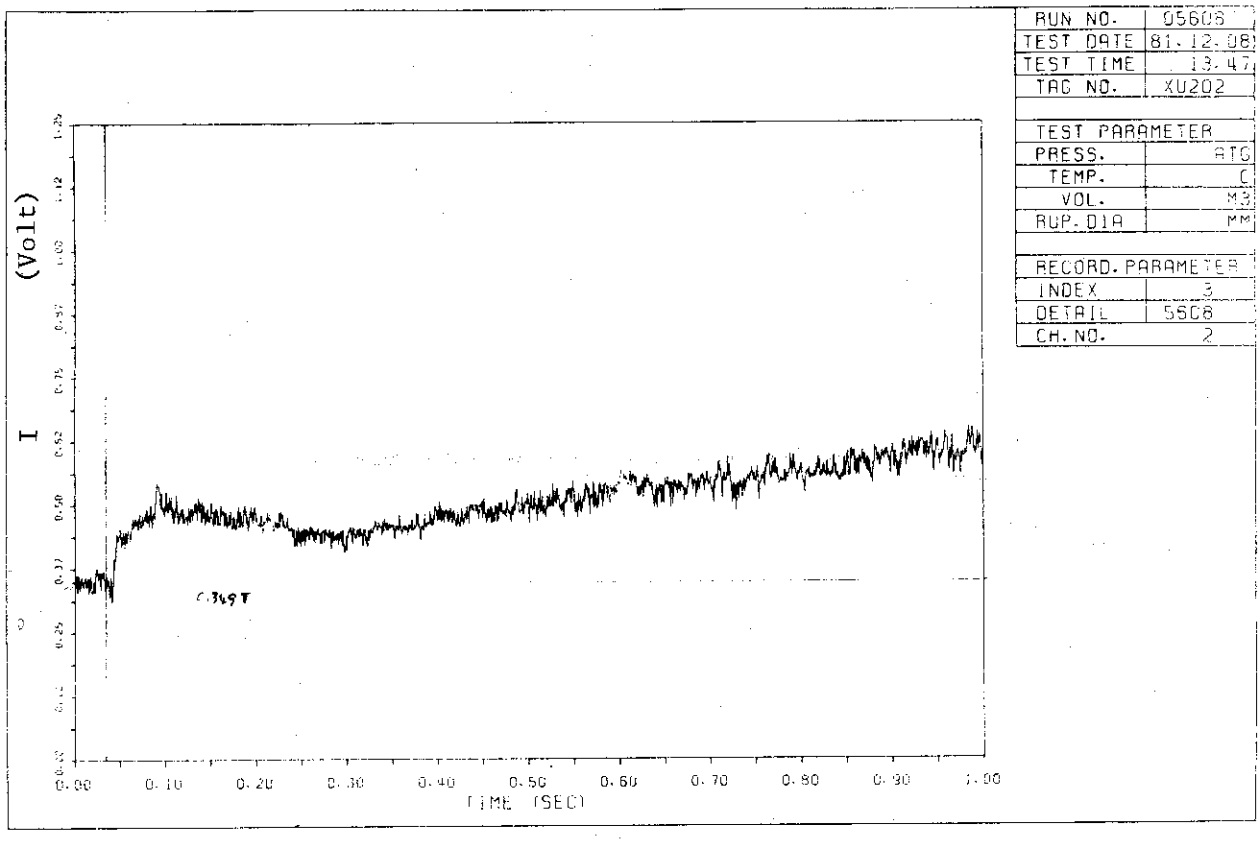

Fig. 19 Output of gamma-ray densitometer, Run 5608, XU202, 0 - 1 sec

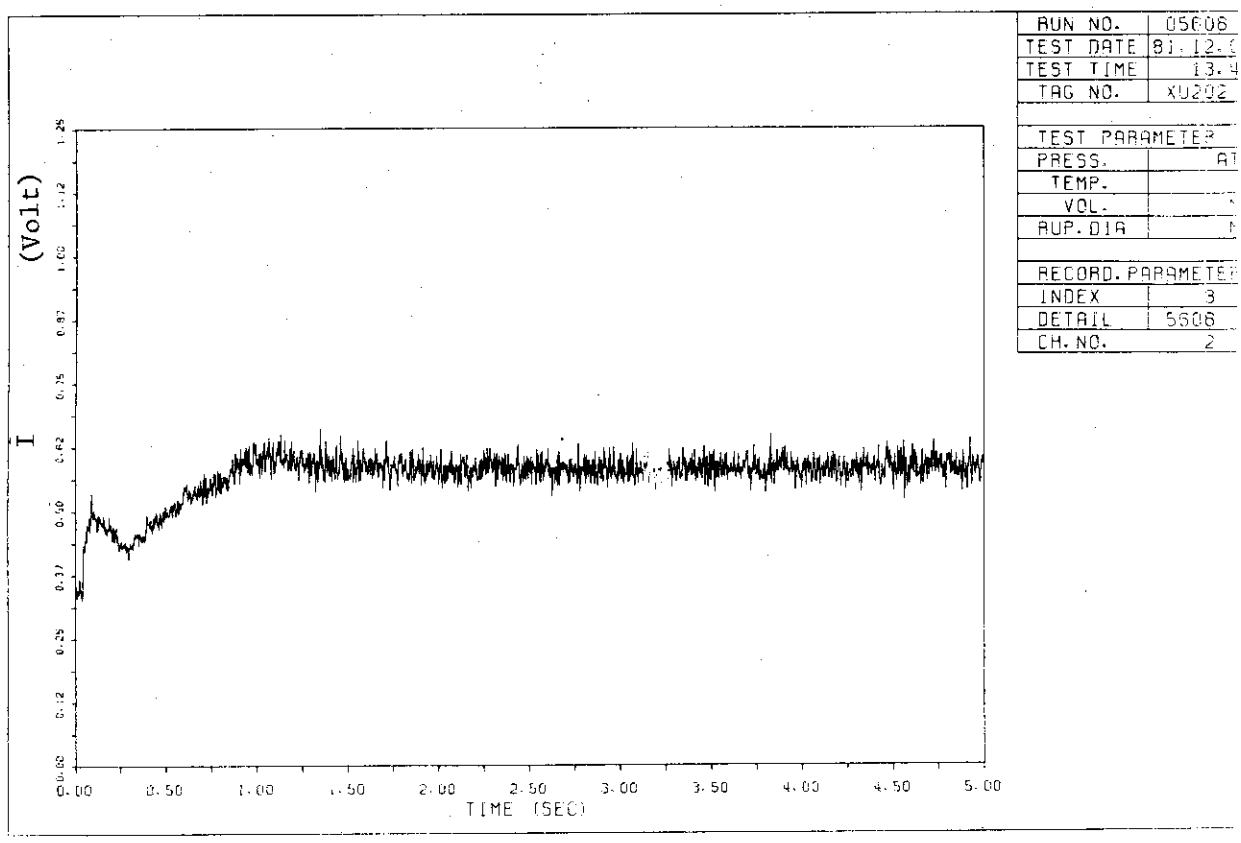

Fig. 20 Output of gamma-ray densitometer, Run 5608, XU202, 0 - 5 sec

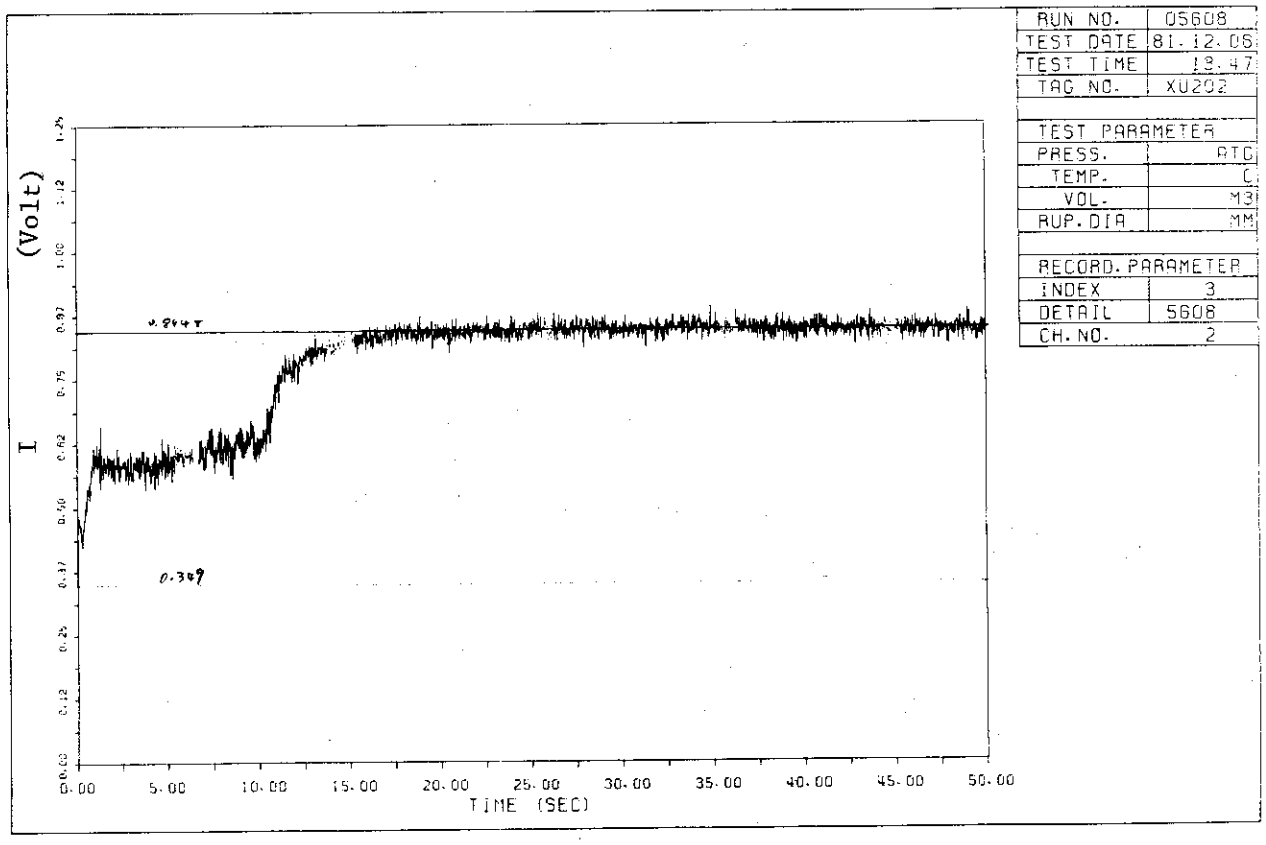

Fig. 21 Output of gamma-ray densitometer, Run 5608, XU202, 0 - 50 sec

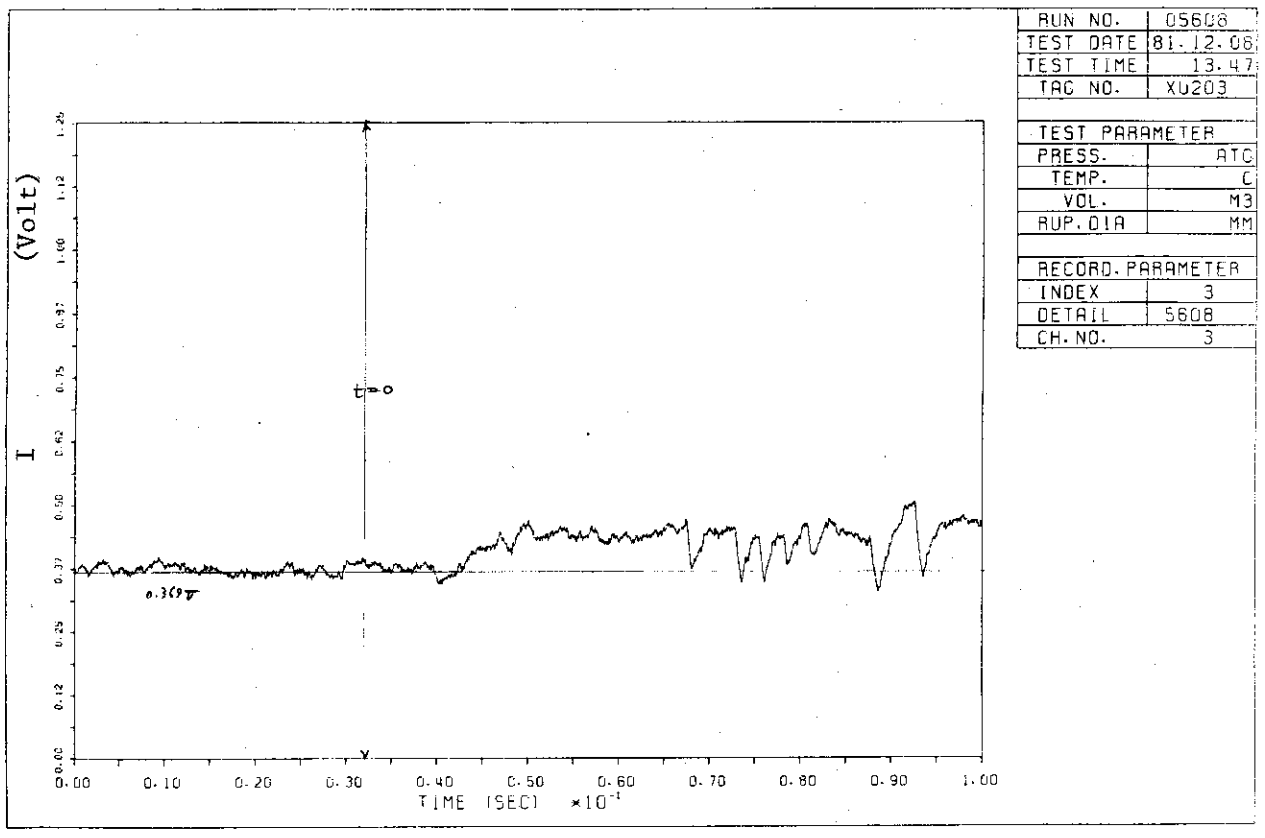

Fig. 22 Output of gamma-ray densitometer, Run 5608, XU203, 0 - 0.1 sec

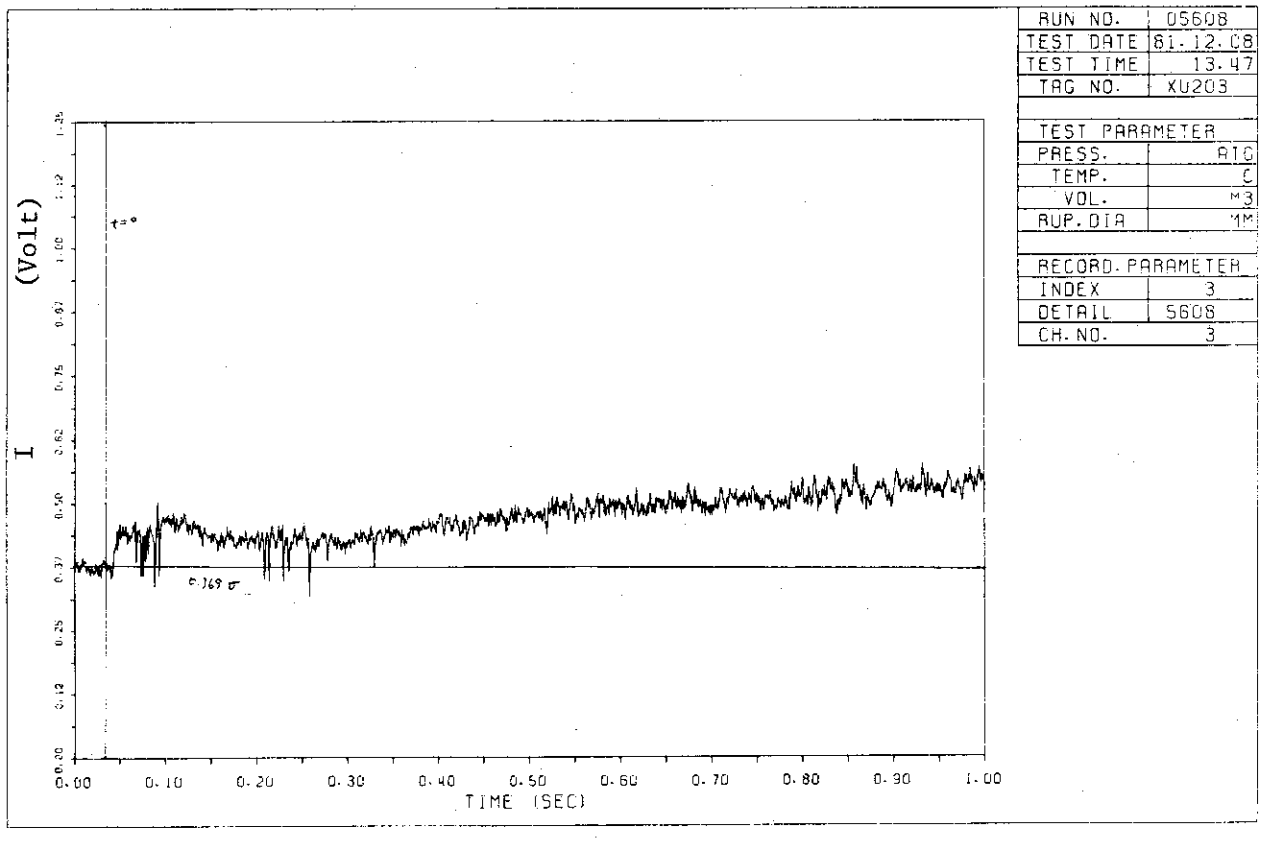

Fig. 23 Output of gamma-ray densitometer, Run 5608, XU203, 0 - 1 sec

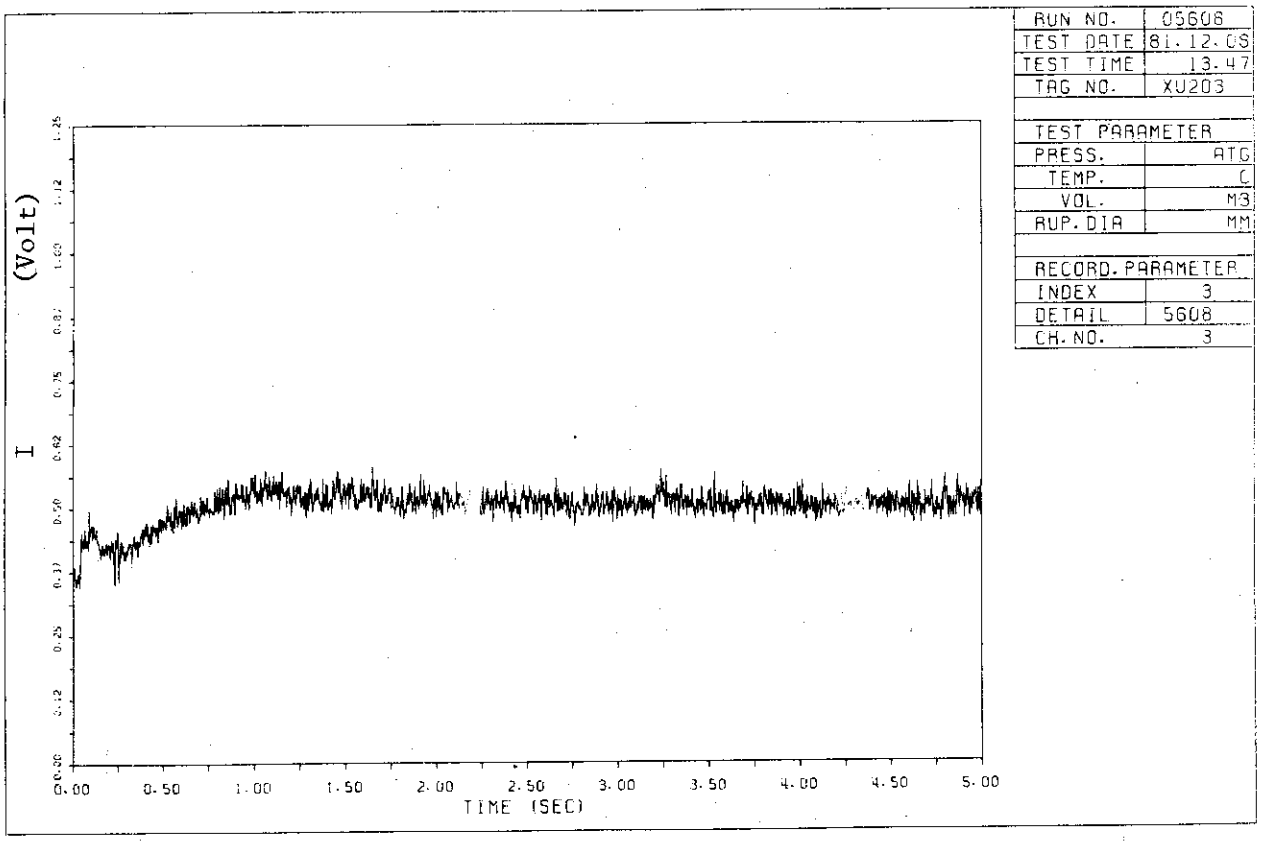

Fig. 24 Output of gamma-ray densitometer, Run 5608, XU203, 0 - 5 sec

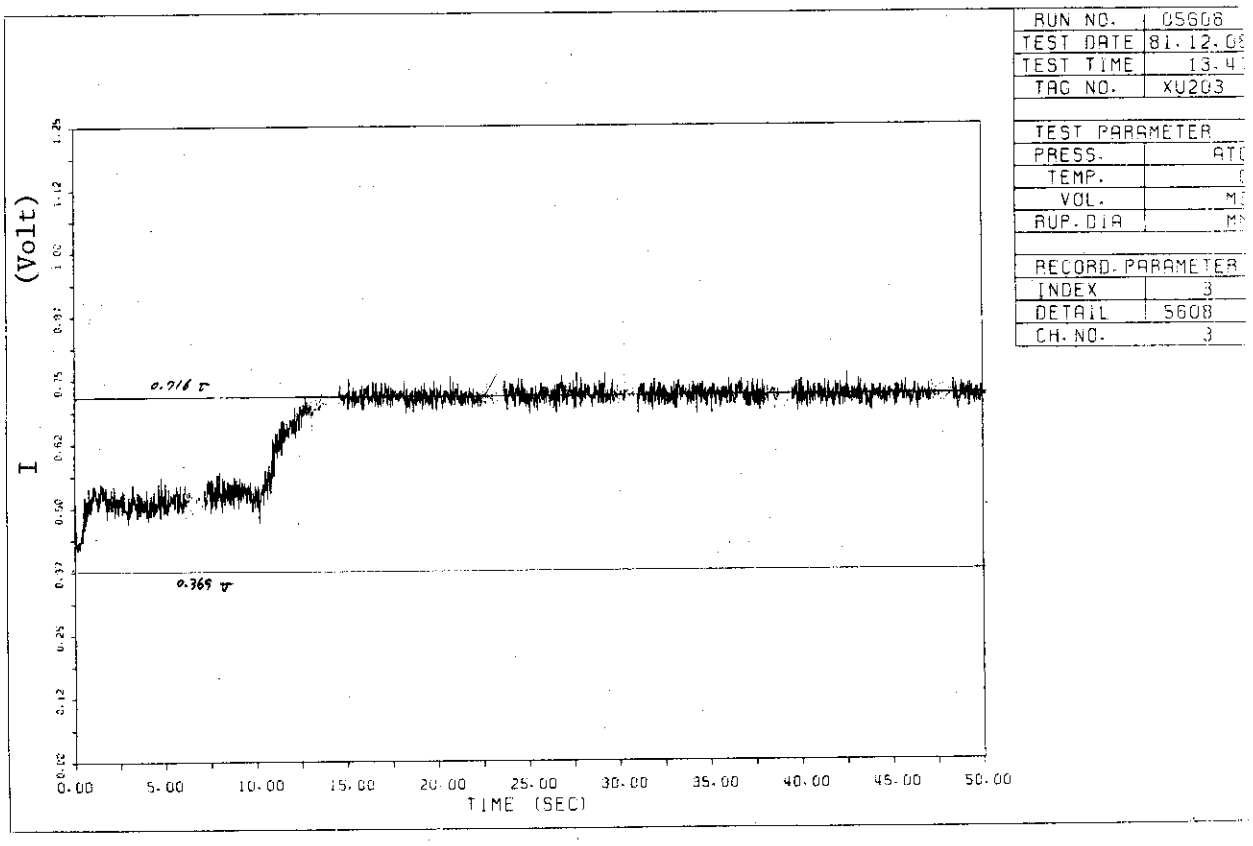

Fig. 25 Output of gamma-ray densitometer, Run 5608, XU203, 0 - 50 sec

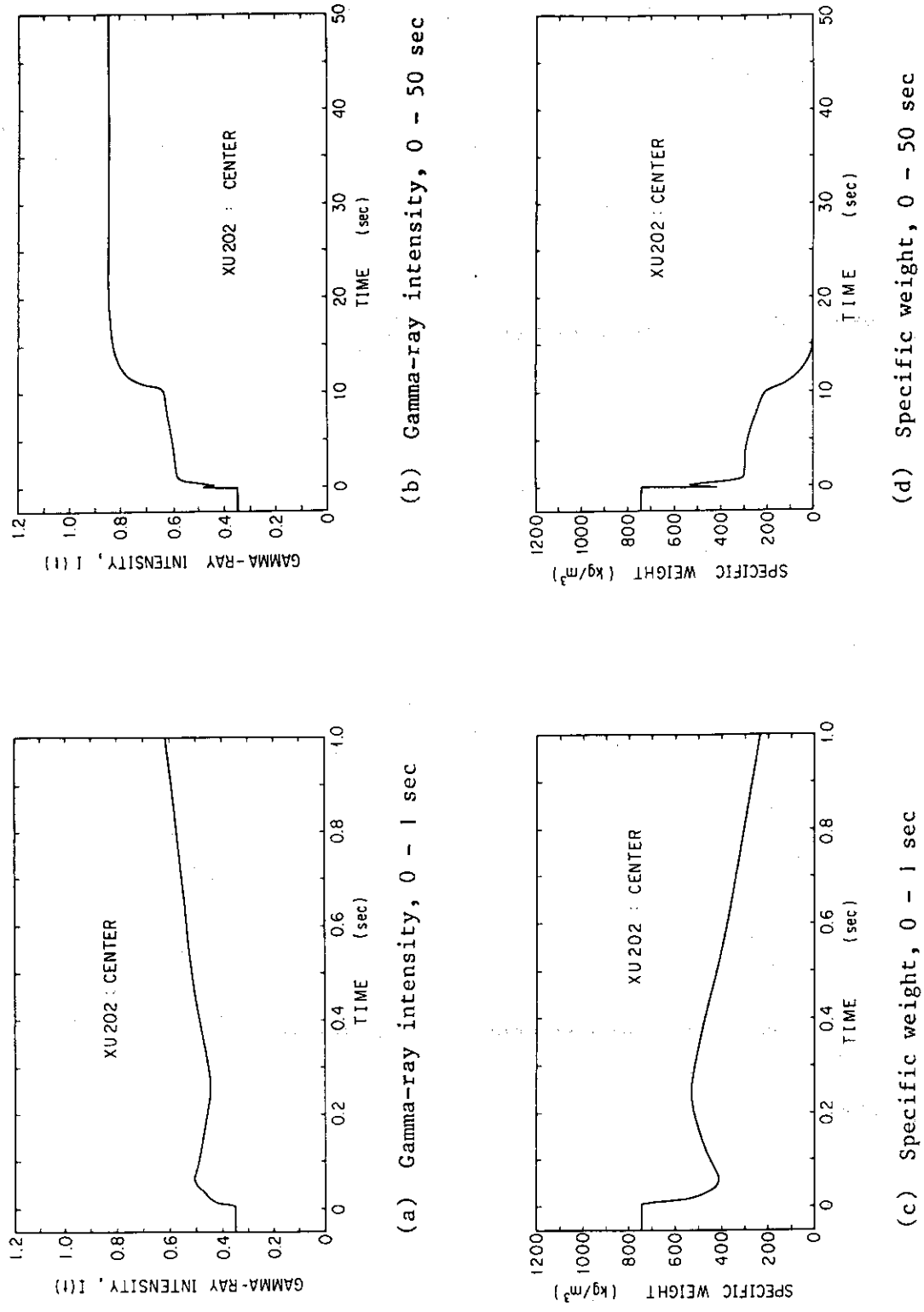

Fig. 26 Measurement in experiment by the center detector, XU202, of three beam gamma-ray densitometer

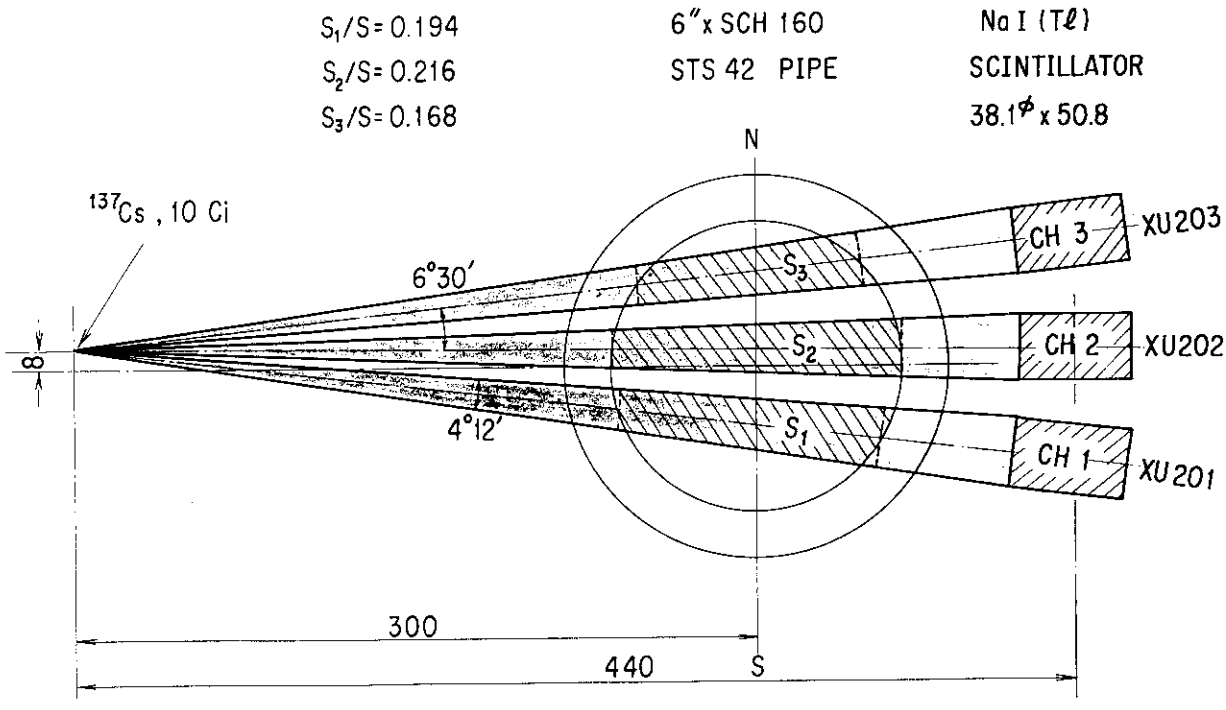

Fig. 27 Conceptual arrangement and cross sections through the pipe of gamma-ray densitometer

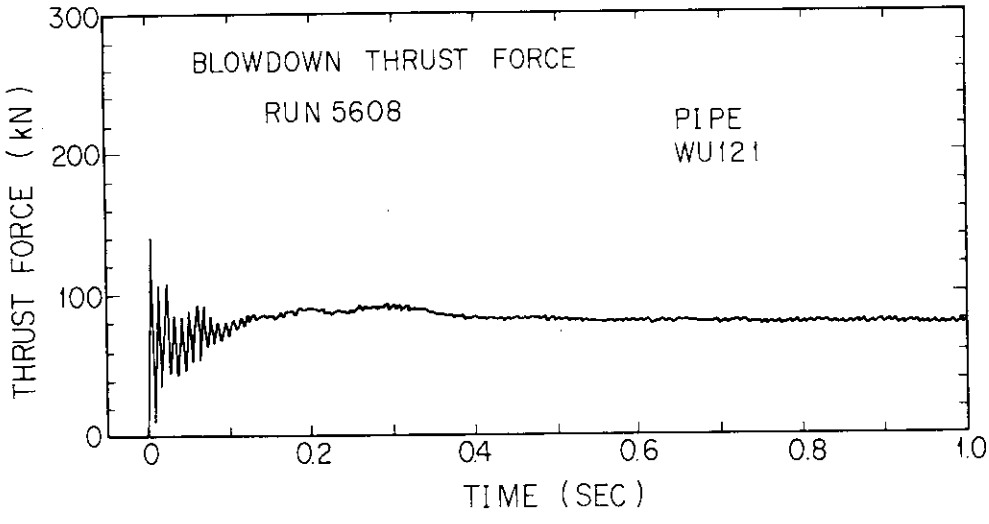

Fig. 29 Blowdown thrust force in the pipe rupture test[3]

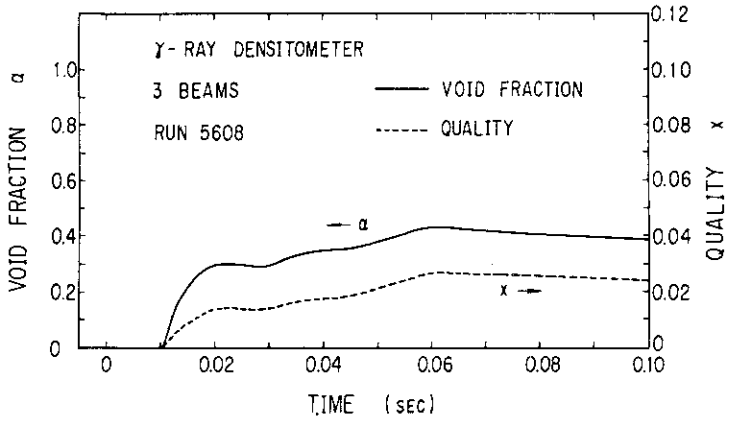

(a) 0 - 0.1 sec

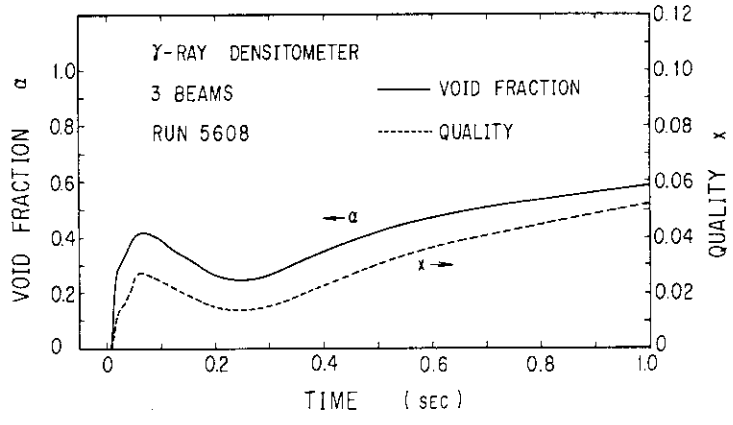

(b) 0 - 1 sec

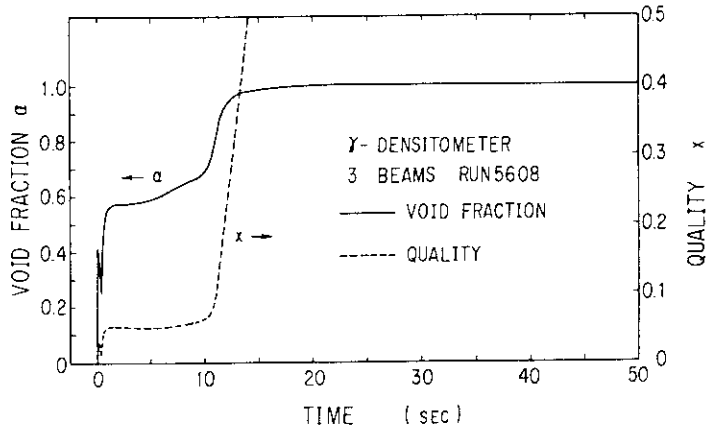

(c) 0 - 50 sec

Fig. 28 Void fraction and quality of flashing water under instantaneous pipe rupture

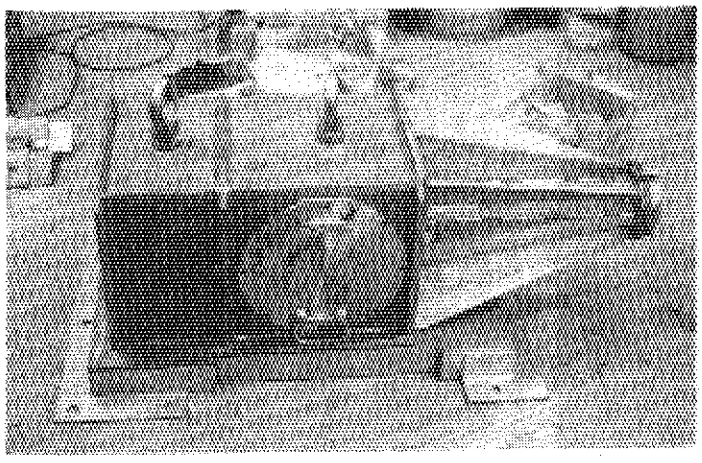

Photo. 1 Gamma-ray source cask

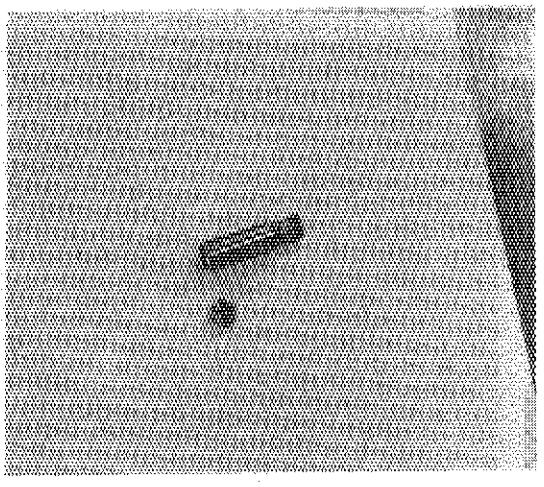

Photo. 3 Capsule of gamma-ray source

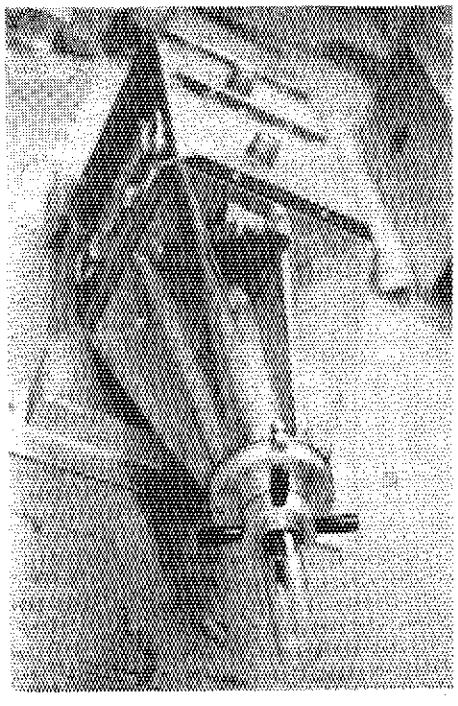

Photo. 2 Source cask, and window of source position indicator

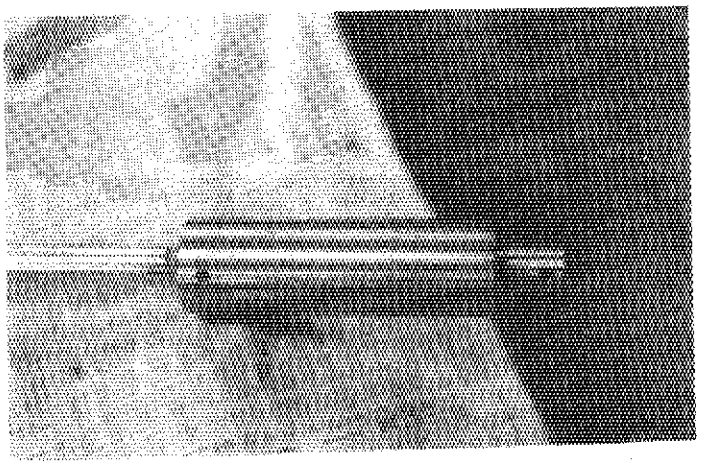

Photo. 4 Movable shield of gamma-ray source capsule

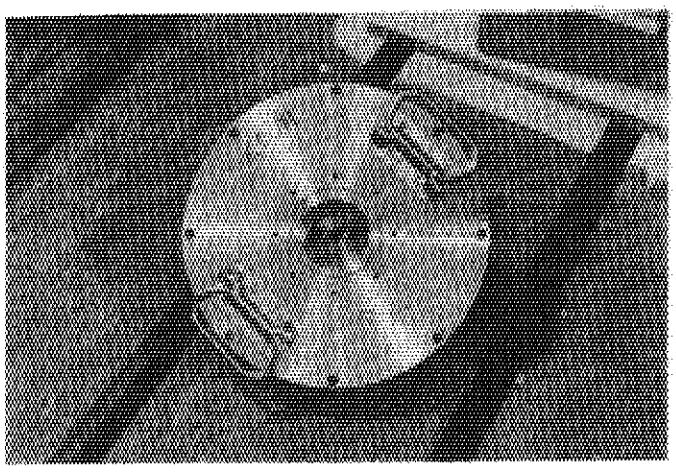

Photo. 5 Outer side of collimator of source cask

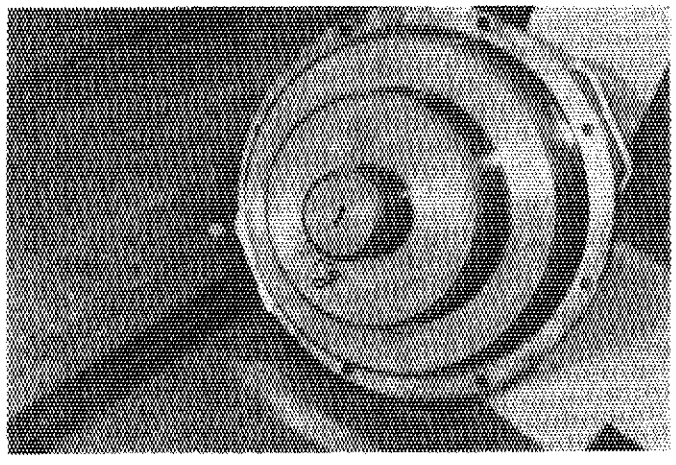

Photo. 6 Inner side of collimator of source cask

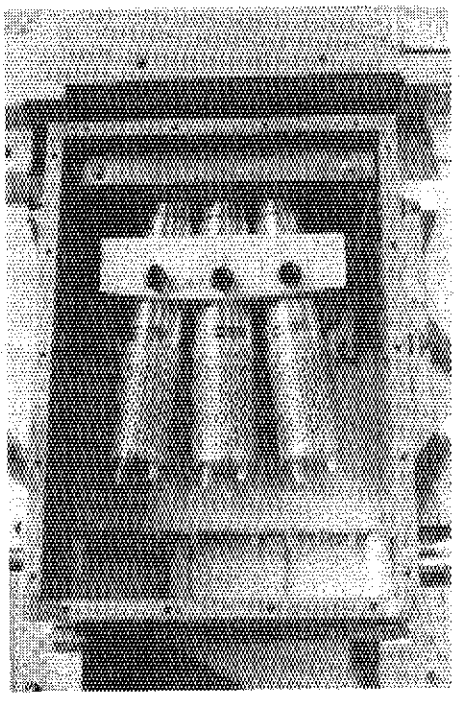

Photo. 7 Detector box and scintillators

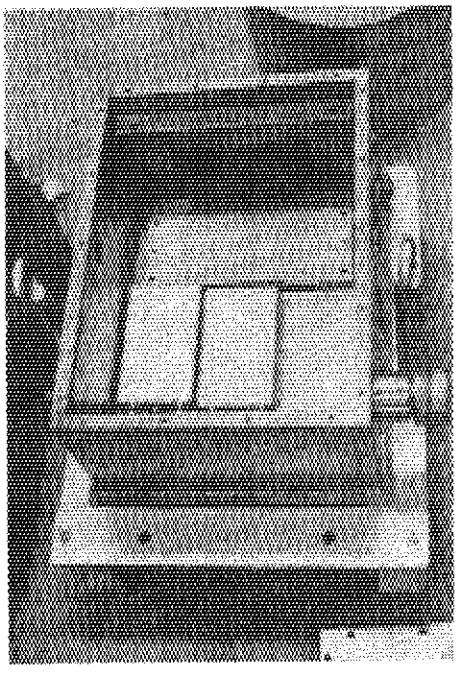

Photo. 8 Detector box and pre-amplifiers

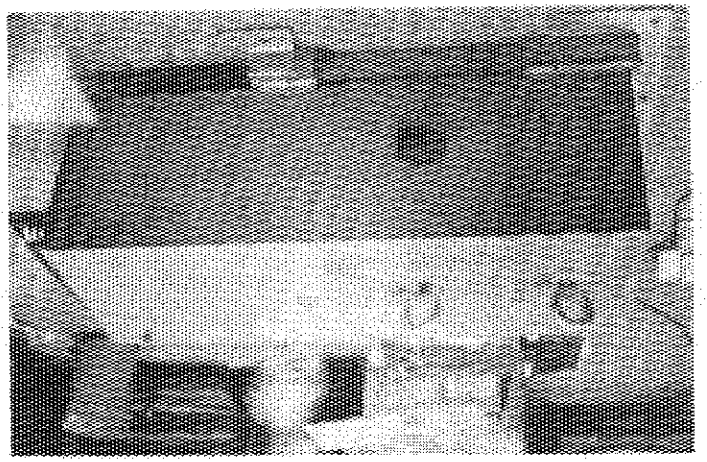

Photo. 9 Water cooling jacket of source cask

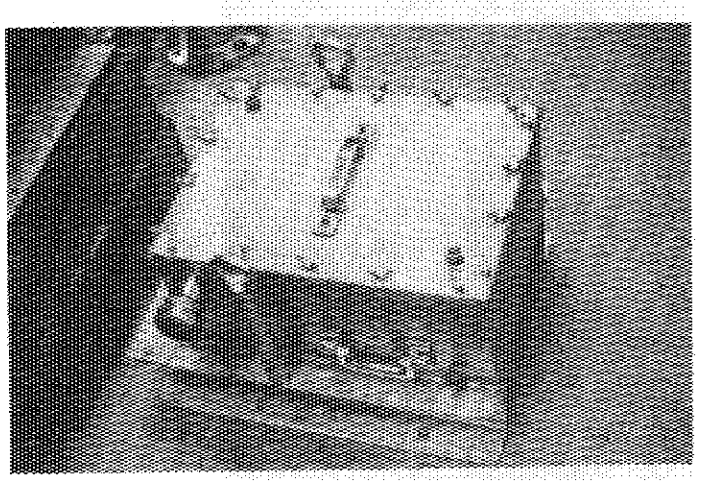

Photo. 10 Water cooling jacket of detector box

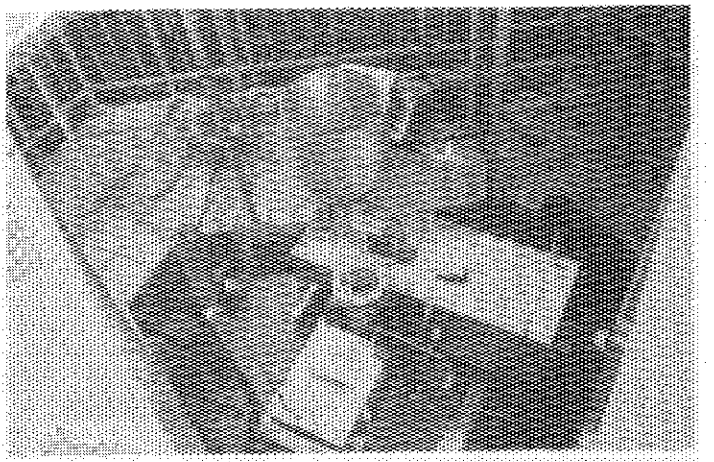

Photo. 11 Apparatus for calibration test

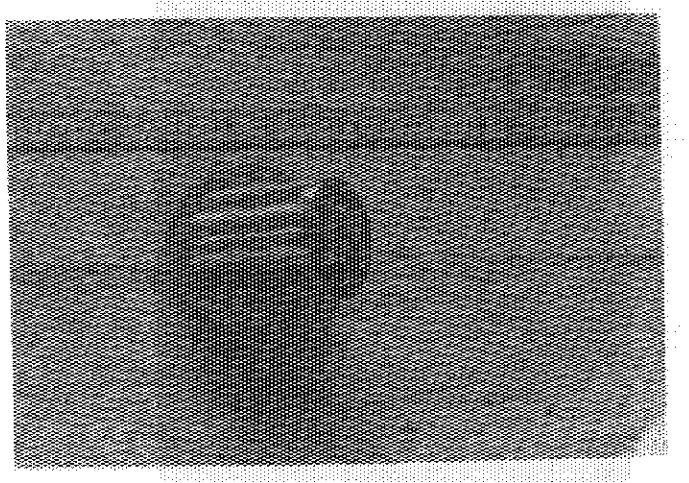

Photo. 12 Acrylic void simulator with 25 % void

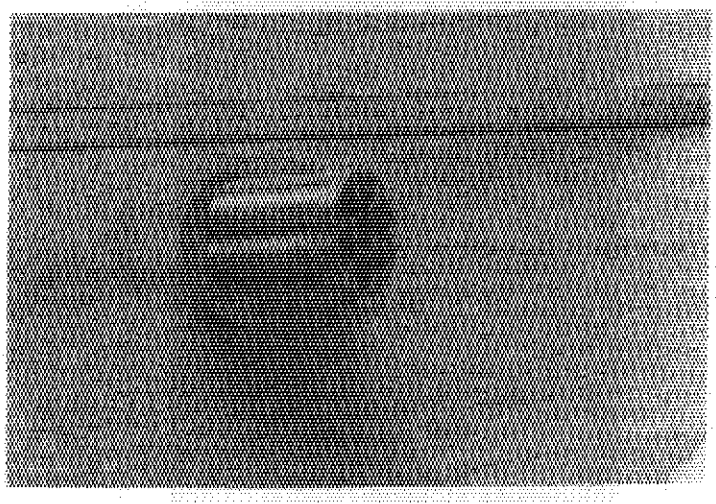

Photo. 13 Acrylic void simulator with 50 % void

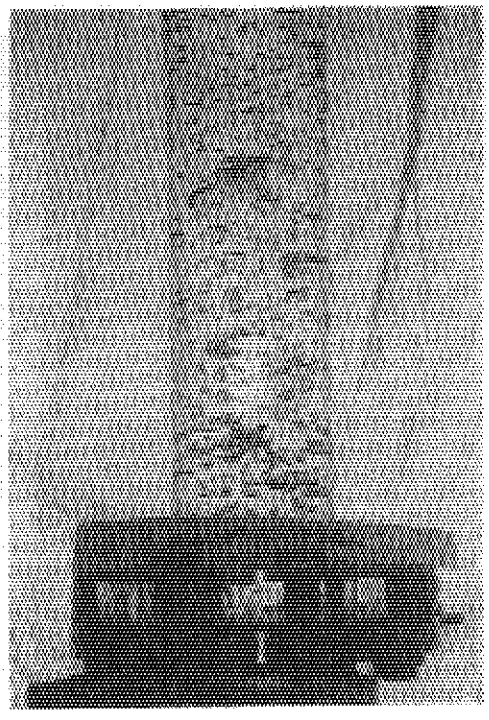

Photo. 15 Bubbly flow in air injection test into cold water

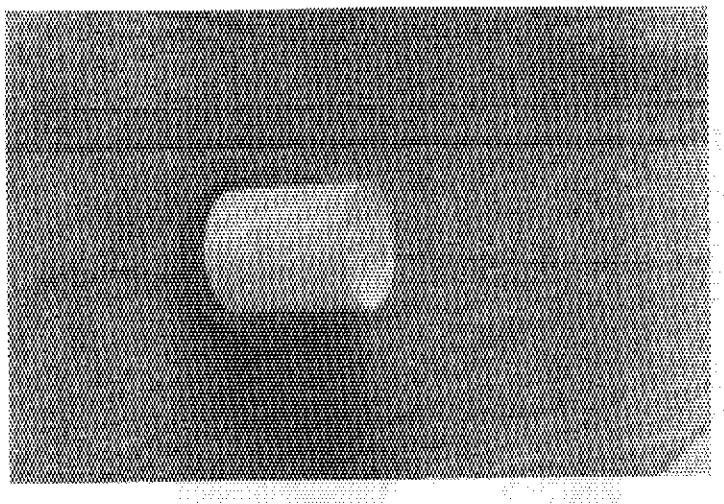

Photo. 14 Acrylic void simulator with 95 % void

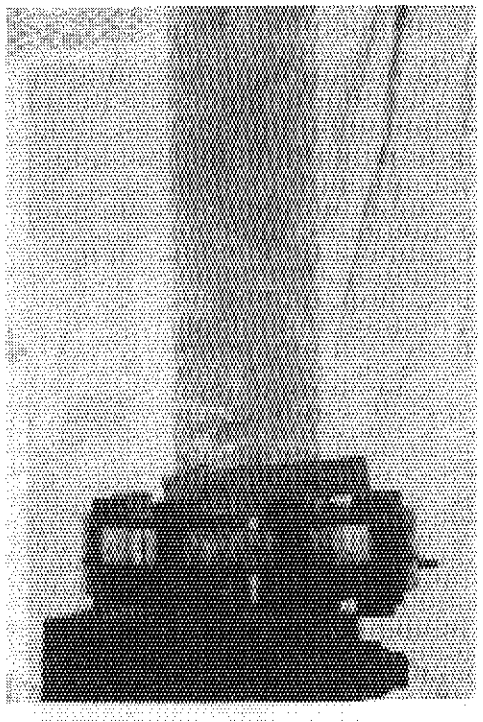

Photo. 16 Slug flow in air injection test into cold water

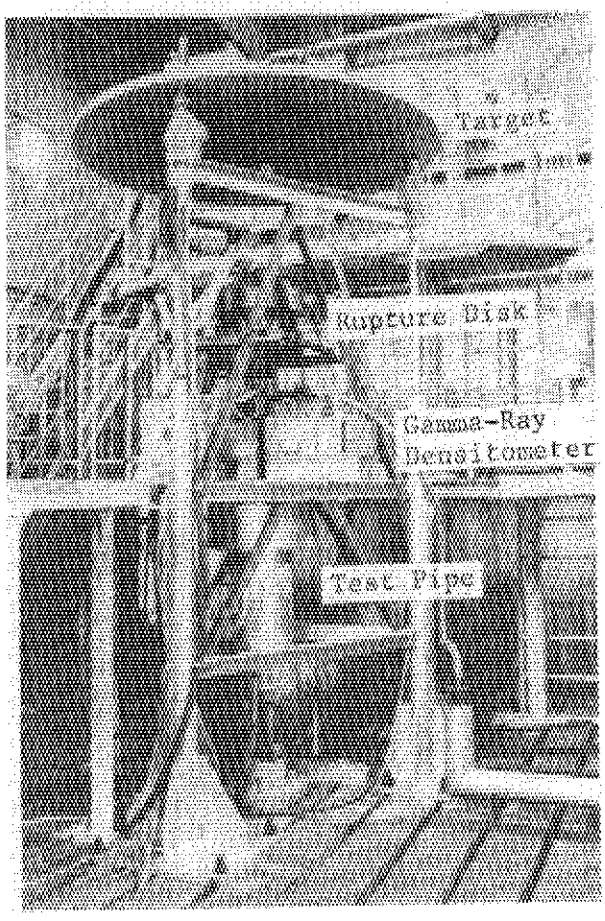

Photo. 17 Apparatus of jet discharge test

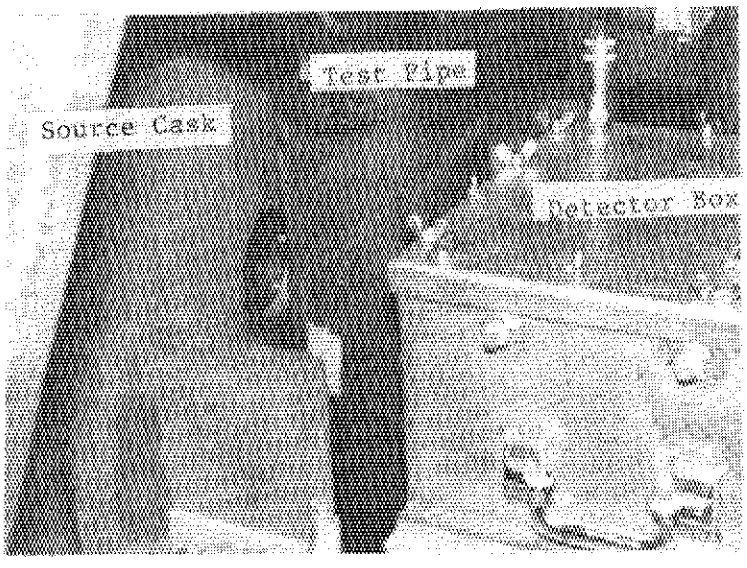

Photo. 18 Arrangement of gamma-ray densitometer